HAL open science

Inertial Sensitivity of Porous Microstructures

Martin Pauthenet, Yohan Davit, Michel Quintard, Alessandro Bottaro

To cite this version:

Martin Pauthenet, Yohan Davit, Michel Quintard, Alessandro Bottaro. Inertial Sensitivity of Porous Microstructures. Transport in Porous Media, 2018, 125 (2), pp.211-238. 10.1007/s11242-018-1115-1 . hal-02391925

HAL Id: hal-02391925

https://hal.science/hal-02391925v1

Submitted on 2 Feb 2024

HAL is a multi-disciplinary open access archive for the deposit and dissemination of scientific research documents, whether they are published or not. The documents may come from teaching and research institutions in France or abroad, or from public or private research centers.

L'archive ouverte pluridisciplinaire **HAL**, est destinée au dépôt et à la diffusion de documents scientifiques de niveau recherche, publiés ou non, émanant des établissements d'enseignement et de recherche français ou étrangers, des laboratoires publics ou privés.

Open Archive Toulouse Archive Ouverte

OATAO is an open access repository that collects the work of Toulouse researchers and makes it freely available over the web where possible

This is an author's version published in: http://oatao.univ-toulouse.fr/20719

Official URL:

https://doi.org/10.1007/s11242-018-1115-1

To cite this version:

Pauthenet, Martin and Davit, Yohan and Quintard, Michel and Bottaro, Alessandro Inertial Sensitivity of Porous Microstructures. (2018) Transport in Porous Media, 125 (2). 211-238. ISSN 0169-3913

Any correspondence concerning this service should be sent to the repository administrator: tech-oatao@listes-diff.inp-toulouse.fr

Inertial Sensitivity of Porous Microstructures

Martin Pauthenet[1] · Yohan Davit[1] · Michel Quintard[1] · Alessandro Bottaro[1,2]

Received: 13 October 2017 / Accepted: 6 July 2018 / Published online: 11 July 2018

Abstract

Fluid flows through porous media are subject to different regimes, ranging from linear creeping flows to unsteady, chaotic turbulence. These different flow regimes at the pore scale have repercussions at larger scales, with the macroscale drag force experienced by a fluid moving through the medium becoming a nonlinear function of the average velocity beyond the creeping flow regime. Accurate prediction of the transition between different flow regimes is an important challenge with repercussions onto many engineering applications. Here, we are interested in the first deviation from Darcy's law, when inertia effects become sizeable. Our goal is to define a Reynolds number, Re_C, so that the inertial deviation occurs when $Re_C \sim 1$ for any microstructure. The difficulty in doing so is to reduce the multiple length scales characterizing the geometry of the porous structure to a single length scale, ℓ. We analyze the problem using the method of volume averaging and identify a length scale in the form $\ell = C_\lambda \sqrt{K_\lambda / \epsilon_\beta}$, with C_λ a parameter that indicates the sensitivity of the microstructure to inertia. The main advantage of this definition is that an explicit formula for C_λ is given; C_λ is computed from a creeping flow simulation in the porous medium; and Re_C can be used to predict the transition to a non-Darcian regime more accurately than by using Reynolds numbers based on alternative length scales. The theory is validated numerically with data from flow simulations for a variety of microstructures.

Keywords Volume-averaging method · Filtration law · Inertial flow · Reynolds number

List of Symbols

$\bullet_\beta$	Item related to the fluid phase (β-phase)
C_λ	Inertial sensitivity of the microstructure
ϵ_β	Porosity
ℓ	Length scale used in Re_C (L)
ℓ_β	Pore length scale (L)
$F_\parallel$, $F_\perp$	Parallel and orthogonal Forchheimer terms
F_λ	Forchheimer number

✉ Martin Pauthenet
martin.pauthenet@imft.fr

1 Institut de Mécanique des Fluides de Toulouse (IMFT), Université de Toulouse, CNRS, Toulouse, France

2 DICCA, Scuola Politecnica University of Genova, 1 Via Montallegro, 16145 Genoa, Italy

γ_β	β-phase indicator
$\mathbf{g}_\beta$	Macroscopic pressure gradient ($\mathrm{ML^{-2}T^{-2}}$)
K_λ	Scalar permeability ($\mathrm{L^2}$)
$\boldsymbol{\lambda}$	Direction of the intrinsic average velocity
$\mathscr{A}_{\beta\sigma}$	Domain of the fluid–solid interface
$\mathscr{V}$	Domain of the REV
$\mathscr{V}_\beta$	Domain of the β-phase
μ_β	Dynamic viscosity of the fluid ($\mathrm{ML^{-1}T^{-1}}$)
ν_β	Kinematic viscosity of the fluid ($\mathrm{L^2T^{-1}}$)
p_β	Pressure field ($\mathrm{ML^{-2}T^{-2}}$)
ψ	Generic field
$\mathbb{R}$	Real space
Re_C, Re_k	Critical- and permeability-based Reynolds number
ρ_β	Density of the fluid ($\mathrm{ML^{-3}}$)
ℓ_0	Dimension of the REV (L)
$\mathbf{v}_\beta$	Flow velocity field ($\mathrm{LT^{-1}}$)
$\mathbf{f}$	Extension of Darcy's law ($\mathrm{L^{-2}}$)
$\mathbf{K}_\mathrm{D}$	Darcy permeability ($\mathrm{L^2}$)
$\mathbf{r}$	General position vector (L)
$\mathbf{s}_\beta$	Constant source term ($\mathrm{LT^{-2}}$)
$\mathbf{y}_\beta = \mathbf{r} - \mathbf{x}$	Position vector relative to the centroid of the REV (L)
$\langle \mathbf{v}_\beta \rangle^\beta$, $\langle p_\beta \rangle^\beta$	Intrinsic averages
$\tilde{\mathbf{v}}_\beta$, $\tilde{p}_\beta$	Spatial deviations
$\mathbf{v}^*$, p^*	Dimensionless spatial deviations
b	Nonlinear part of Ergun's equation ($\mathrm{L^{-1}T}$)
L_v	Macroscopic length scale (L)
V	Measure of the REV ($\mathrm{L^3}$)
v	Magnitude of the intrinsic average velocity ($\mathrm{LT^{-1}}$)
V_β	Measure of the β-phase inside the REV ($\mathrm{L^3}$)

1 Introduction

A fluid flowing through a porous medium experiences three main transition phenomena with increasing flow rate (Schneebeli 1955; Chauveteau and Thirriot 1967; Dybbs and Edwards 1984; Fand et al. 1987; Seguin et al. 1998a, b; Lage 1998; Venkataraman and Rao 1998; Hlushkou and Tallarek 2006). The first one is a transition from the creeping flow regime to the non-Darcian, inertial steady regime. Then, the flow evolves to successive unsteady regimes. The last transition occurs when turbulence appears, characterized by unsteady, chaotic flow features in the porous medium. This latter regime presents several open modeling issues (Masuoka and Takatsu 1996; Antohe and Lage 1997; Kuwahara et al. 1998; Nakayama and Kuwahara 1999; Chandesris et al. 2006; De Lemos 2012; Jin et al. 2015; Jin and Kuznetsov 2017). Since the filtration law in porous media strongly depends on the flow regime, it is of importance to characterize these transitions. This has applications to natural and as well as industrial systems, including modeling the transport of chemical species (Whitaker 1967; Vafai and Tien 1982; Hoffmann et al. 1997; Souto and Moyne 1997; Wood 2007) and heat (Hong et al. 1987; Amiri and Vafai 1994; Goyeau et al. 1996; Quintard et al. 1997; Kim et al. 2000; Aydın and Kaya 2008; Chikhi et al. 2016) in, e.g. , packed-bed column reactors,

soil percolation, microscopic heat exchangers and the fluid–structure coupling in flexible canopies (Ghisalberti and Nepf 2002, 2005; Gosselin 2009; Favier et al. 2009; Gosselin and de Langre 2011).

Under a macroscopic pressure gradient $\mathbf{g}_\beta$,[1] a fluid initially at rest in a porous medium accelerates[2] until the internal viscous dissipation of the flow balances the rate of work of $\mathbf{g}_\beta$. In the steady regime, the flow reaches a state characterized by a spatially averaged velocity $\langle \mathbf{v}_\beta \rangle^\beta$. This velocity can be written as

$$\langle \mathbf{v}_\beta \rangle^\beta = v\boldsymbol{\lambda}, \tag{1}$$

with $\boldsymbol{\lambda}$ the unit vector defining the mean flow direction and v the amplitude of $\langle \mathbf{v}_\beta \rangle^\beta$. To a given $\mathbf{g}_\beta$ corresponds a unique $\langle \mathbf{v}_\beta \rangle^\beta$, and vice versa. We write this as a filtration law, $\mathbf{g}_\beta = \mathbf{g}_\beta(\boldsymbol{\lambda}, v)$. A priori the nature of $\mathbf{g}_\beta(\boldsymbol{\lambda}, v)$ depends on the topology of the porous medium, the flow regime and the physical properties of the fluid (Forchheimer 1901; Carman 1937; Klinkenberg 1941; Ergun 1952; Brace et al. 1968; Jackson and James 1986; Wong et al. 1997).

In "Appendix A.1," we show that for a fluid under constant volume force $\mathbf{s}_\beta$, the macroscopic pressure gradient can be related to the gradient of the intrinsic average pressure $\nabla \langle p_\beta \rangle^\beta$ as

$$\mathbf{g}_\beta = \nabla \langle p_\beta \rangle^\beta - \rho_\beta \mathbf{s}_\beta, \tag{2}$$

where ϵ_β is the porosity of the medium. In the creeping flow regime, $\mathbf{g}_\beta(\boldsymbol{\lambda}, v)$ is Darcy's law (Darcy 1856), which amounts to write

$$\nabla \langle p_\beta \rangle^\beta - \rho_\beta \mathbf{s}_\beta = -\epsilon_\beta \mu_\beta \mathbf{K}_\mathrm{D}^{-1} \cdot \boldsymbol{\lambda} v, \tag{3}$$

where μ_β is the dynamic viscosity of the fluid. The "$\cdot$" symbol in Eq. 3 refers to the usual inner product. $\mathbf{K}_\mathrm{D}$ (a second-order tensor) is the permeability of the porous medium. We can further define a scalar characterizing the permeability for a flow in the $\boldsymbol{\lambda}$ direction as

$$K_\lambda^{-1} = ||\mathbf{K}_\mathrm{D}^{-1} \cdot \boldsymbol{\lambda}||. \tag{4}$$

Beyond the creeping flow regime, nonlinear effects at the pore scale modify the flow pattern, and the filtration law becomes non-Darcian (Hassanizadeh and Gray 1987; Mei and Auriault 1991; Firdaouss et al. 1997; Ma and Ruth 1997; Rojas and Koplik 1998; Skjetne and Auriault 1999; Panfilov et al. 2003; Zimmerman et al. 2004; Lasseux et al. 2011). We can extend Darcy's law as

$$\nabla \langle p_\beta \rangle^\beta - \rho_\beta \mathbf{s}_\beta = -\epsilon_\beta \mu_\beta \left(\mathbf{K}_\mathrm{D}^{-1} \cdot \boldsymbol{\lambda} + \mathbf{f} \right) v. \tag{5}$$

A simple way of characterizing the range of validity of Darcy's law is by considering the Forchheimer number (Ruth and Ma 1992; Andrade et al. 1999; Lage and Antohe 2000; Zeng and Grigg 2006; Muljadi et al. 2016)

$$F_\lambda = \frac{||\mathbf{f}||}{K_\lambda^{-1}}, \tag{6}$$

which is the ratio of the nonlinear to the linear part of the filtration law. Darcy's law remains valid as long as $F_\lambda \ll 1$ and the inertial transition occurs when $F_\lambda \sim 1$.

[1] See Sect. A.1 and Eq. 54 for a detailled derivation of $\mathbf{g}_\beta$ with respect to the microscopic fields.

[2] This initial transient regime is generally neglected in macroscopic models.

To capture the inertial transition a priori, a Reynolds number Re_{C} is of practical interest. Let ν_β be the kinematic viscosity of the fluid ($\mu_\beta = \nu_\beta \rho_\beta$). In general, Re_{C} is expressed as a ratio of the advection time to the viscous diffusion time, in terms of v, ν_β, and a length scale ℓ as

$$Re_{\mathrm{C}} = \frac{\ell v}{\nu_\beta}. \tag{7}$$

The choice of the characteristic length scale to define such a Reynolds number is widely discussed in the literature (Lage and Antohe 2000; Lasseux et al. 2011; Venkataraman and Rao 1998; Beavers and Sparrow 1969; Mcdonald et al. 1979; Philipse and Schram 1991; Li and Ma 2011a, b; Muljadi et al. 2016). For a given porous medium, ℓ should be easy to identify, and such that Re_{C} past a well-defined threshold indicates the inertial transition. A simple choice for ℓ is a characteristic pore size ℓ_β (Amiri and Vafai 1994; Li and Ma 2011a, b; Andrade et al. 1995; Clavier et al. 2015, 2017). However, such a microscopic length scale may not be well defined for porous media that exhibit non-trivial or complex microstructures, such as sandstones.

If we have an explicit filtration law, we can use the Forchheimer number as a Reynolds number (Andrade et al. 1999; Lage and Antohe 2000; Zeng and Grigg 2006). For example, the classical filtration law (Ergun's equation, Ergun 1952) takes into account inertia effect on the filtration law via a quadratic form. For a one-dimensional filtration process, this quadratic filtration law is a scalar relation given by

$$g_\beta\left(\boldsymbol{\lambda}, v\right) = \epsilon_\beta \mu_\beta K_\lambda^{-1}\left(1 + bv\right) v. \tag{8}$$

Inertia effects are small as long as the quadratic part is small against the linear part. Taking the ratio of the quadratic part to the linear part (i.e. , $\frac{bv}{1}$), and identifying it with Re_{C}, i.e. ,

$$\frac{bv}{1} = \frac{\ell v}{\nu_\beta}, \tag{9}$$

we obtain ℓ as

$$\ell = b\nu_\beta. \tag{10}$$

This means that if we use this expression for the characteristic length scale ℓ in Eq. 7, Re_{C} compares directly the relative influence of the linear and inertial contributions in the macroscopic filtration law. Unfortunately in practice, either experiments or direct numerical simulations (DNS) are needed to determine the parameter b. Moreover, Eq. 8 assumes a quadratic form, which is questionable when going from the linear to the nonlinear regime (Mei and Auriault 1991; Firdaouss et al. 1997; Rojas and Koplik 1998; Skjetne and Auriault 1999; Clavier et al. 2015; Wodie and Levy 1991; Lucas et al. 2007). In Sect. 3.2.1 we propose an expression for the Forchheimer number.

Yet another possibility is the use of a permeability-based Reynolds number (Beavers and Sparrow 1969; Vafai and Tien 1981; Nield and Bejan 1999; Papathanasiou et al. 2001; Dukhan et al. 2014; Muljadi et al. 2016) defined as

$$Re_{\mathrm{k}} = v\frac{\sqrt{K_\lambda/\epsilon_\beta}}{\nu_\beta}. \tag{11}$$

One of the main advantages of this definition is that $\ell = \sqrt{K_\lambda/\epsilon_\beta}$ is not a pure geometrical length scale. ℓ defined as such is associated with Stokes flow in the specific structure of interest and characterizes the overall viscous dissipation in the porous medium. Therefore, $\ell = \sqrt{K_\lambda/\epsilon_\beta}$ should be much better than a geometrical pore length scale at characterizing

viscous effects for the purpose of comparing them to inertial effects, which is the point of a Reynolds number. Unfortunately, even Re_{k} is inaccurate in predicting the inertial deviation, as will be shown later on for a variety of porous structures (Sect. 3.2.2). An obvious example of this is the case of cylindrical pores, for which the non-Darcian, steady regime simply does not exist (Skjetne and Auriault 1999). This is due to the fact that in cylindrical pores, the streamlines (i.e. , lines that are parallel to the $\mathbf{v}_\beta$-field) are locally orthogonal to velocity gradients $\nabla \mathbf{v}_\beta$. Under such circumstances, in the momentum part of the Navier–Stokes equations

$$\underbrace{\mathbf{v}_\beta \cdot \nabla \mathbf{v}_\beta}_{\text{advective term}} = -\frac{1}{\rho_\beta} \nabla p_\beta + \nu_\beta \nabla^2 \mathbf{v}_\beta + \mathbf{s}_\beta, \tag{12}$$

the advective term vanishes identically, canceling inertia effects. In this case the Navier–Stokes equations reduce to the linear Stokes equations, until the first transition to a non-Darcian, unsteady turbulent regime, which is due to a flow instability that starts several orders of magnitude beyond the stage $Re_{\mathrm{k}} = 1$ (e.g. , Sharp and Adrian 2004).

In this paper, we use the framework of volume averaging to derive a filtration law for weakly inertial flows in periodic porous media. We carefully define the volume-averaging operator and apply it to the Navier–Stokes equations in the porous medium. We make a separation of scales assumption to derive the volume-averaged equations, which are closed by a model of the average hydrodynamic force. This requires the modeling of small scale fields and leads to a closure problem (CP) over a representative elementary volume (REV).

We further use the CP to derive the expression for the Reynolds number, Re_{C}. We proceed by evaluating the order of magnitude of the advective term in the CP, and this allows us to correct Re_{k} with a new parameter C_λ, thus yielding Re_{C}. C_λ characterizes the likeliness of the flow in the microstructure to deviate from Darcy's law and is thus the *inertial sensitivity* of the microstructure. The filtration law is evaluated from direct numerical simulations (DNS) on a variety of porous structures, and it is shown that Re_{C} is much better suited than Re_{k} to predict the non-Darcian transition and resolves the pathological case of cylindrical pores. We finally use this new scaling to derive a generalized Forchheimer law in a highly anisotropic porous medium.

2 Nonlinear Effects

In this section, we propose a framework to study the effect of inertia on the filtration law of a porous medium.

2.1 Pore Scale Flow Model

We consider a rigid periodic porous medium, saturated with a Newtonian fluid. We call β the fluid phase and σ the solid phase within the domain, cf. Fig. 1. We focus on steady and incompressible flows as a response to a constant source term $\mathbf{s}_\beta$. Hence, the fluid phase is driven by the steady Navier–Stokes equations, i.e. ,

$$\nabla \cdot \left(\mathbf{v}_\beta \mathbf{v}_\beta\right) = -\tfrac{1}{\rho_\beta} \nabla p_\beta + \nu_\beta \nabla^2 \mathbf{v}_\beta + \mathbf{s}_\beta, \tag{13a}$$

$$\nabla \cdot \mathbf{v}_\beta = 0, \tag{13b}$$

$$\mathbf{v}_\beta = 0 \text{ at } \mathscr{A}_{\beta\sigma}, \tag{13c}$$

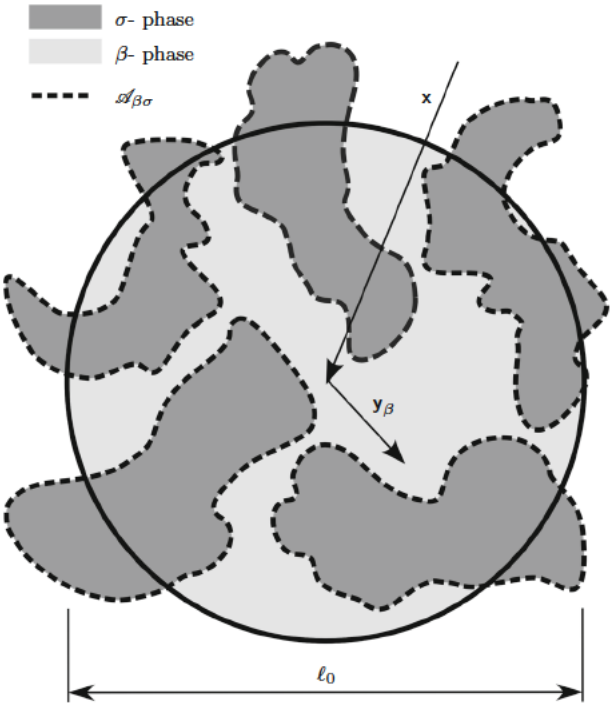

Fig. 1 Averaging volume

with ρ_β the density of the fluid. No-slip conditions are imposed on the fluid–solid interface $\mathscr{A}_{\beta\sigma}$.

Upscaling the Navier–Stokes equations through volume averaging has already received much attention in the literature (see, e.g. , Lasseux et al. 2011; Whitaker 1996; Lasseux and Valdés-Parada 2017). Our development is slightly different in terms of the representation of the spatial deviations (the linear mapping in the cited literature is inconsistent with modeling microscopic inertial effects) and the construction of the anisotropic inertial correction to Darcy's law. The complete derivation provided in "Appendix A" leads to Eq. 65 that we recall here

$$\frac{\ell^2}{\mu_\beta}\mathbf{g}_\beta\left(\boldsymbol{\lambda},\delta\right) = -\mathbf{h}^* v. \tag{14}$$

Depending on v, the equation above yields the macroscopic pressure drop $\mathbf{g}_\beta$ for a steady inertial flow in the $\boldsymbol{\lambda}$ direction. The issue now is to determine $\mathbf{h}^*$ from Eq. 64.

We intend to study the effect of inertia on this filtration law. To characterize the evolution of $\mathbf{h}^*$ due to a flow in the $\boldsymbol{\lambda}$ direction, we build a frame of reference with $\boldsymbol{\lambda}$ and two orthogonal unit vectors $(\mathbf{n}_1, \mathbf{n}_2)$, such that

$$\mathbf{n}_1 \times \mathbf{n}_2 = \boldsymbol{\lambda}, \tag{15}$$

where $\times$ denotes the usual vector product. In this frame, we decompose $\mathbf{f}$ (see Eq. 5), the correction to Darcy's law, into a drag component, $F_\parallel$ and an orthogonal component, $F_\perp$, with ω the angle between the orthogonal term of $\mathbf{f}$ and $\mathbf{n}_1$. These quantities may be expressed as

$$F_{\parallel} = \frac{\boldsymbol{\lambda}\cdot\mathbf{f}}{K_{\lambda}^{-1}}, \tag{16a}$$

$$F_{\perp} = \left\| (\mathbf{I} - \boldsymbol{\lambda}\boldsymbol{\lambda}) \cdot \frac{\mathbf{f}}{K_{\lambda}^{-1}} \right\|, \tag{16b}$$

$$\omega = \left((\mathbf{I} - \boldsymbol{\lambda}\boldsymbol{\lambda}) \cdot \frac{\mathbf{g}_{\beta}}{\epsilon_{\beta}\mu_{\beta}K_{\lambda}^{-1}v}, \mathbf{n}_1 \right). \tag{16c}$$

The triplet $(F_{\parallel}, F_{\perp}, \omega)$ completely determines $\mathbf{f}$ according to the relation

$$\mathbf{f} = K_{\lambda}^{-1}\left(F_{\parallel}\boldsymbol{\lambda} + F_{\perp}\left(\cos(\omega)\,\mathbf{n}_1 + \sin(\omega)\,\mathbf{n}_2\right)\right). \tag{17}$$

The advantage of the decomposition expressed by Eq. 16 will become clear in the following.

2.2 Asymptotic Analysis

In this section, we want to check that the form of our closure problem is compatible with results from the literature (Mei and Auriault 1991; Firdaouss et al. 1997; Wodie and Levy 1991). The end result of our analysis here is an asymptotic generalized Forchheimer law (AGF); the developments starts with the identification of a parameter δ given by

$$\delta = \frac{\ell}{\nu_{\beta}}v, \tag{18}$$

and with the search of an asymptotic form of Eq. 14 when $\delta \ll 1$. According to Eq. 64, we assume that the $\mathbf{v}^*$ and p^* fields can be approximated as

$$\mathbf{v}^* = \mathbf{v}_0^* + \delta\mathbf{v}_1^* + \delta^2\mathbf{v}_2^* + O\left(\delta^3\right), \tag{19a}$$

$$p^* = p_0^* + \delta p_1^* + \delta^2 p_2^* + O\left(\delta^3\right). \tag{19b}$$

This yields

$$\mathbf{f} = \sum_{i\geq 0}^{N}\mathbf{f}^{(i)}\delta^i, \text{ with } \mathbf{f}^{(i)} = \mathbf{K}_{\mathrm{D}}^{-1}\cdot\left\langle\mathbf{v}_{i0}^*\right\rangle^{\beta}, \tag{20}$$

where $\mathbf{v}_{i0}^*$ are solutions of Stokes problems (see "Appendix B"). This yields the asymptotic form of Eq. 14

$$\mathbf{g}_{\beta} = -\epsilon_{\beta}\mu_{\beta}\mathbf{K}_{\mathrm{D}}^{-1}\cdot\left(\boldsymbol{\lambda} - \sum_{i\geq 1}^{N}\left\langle\mathbf{v}_{i0}^*\right\rangle^{\beta}\delta^i\right)v, \tag{21}$$

which is our asymptotic generalized Forchheimer law. In Sect. 3, the AGF expressed in Eq. 21 is compared with data from DNS for different microstructures.

Numerical and experimental evidences (Rojas and Koplik 1998; Skjetne and Auriault 1999; Clavier et al. 2015; Lucas et al. 2007) indicate that $\mathbf{f}^{(1)}$ vanishes, leading to a first cubic correction to Darcy's law. This regime is referred to as the *cubic regime*, or *weak inertia regime*, and was studied by two-scale asymptotics (Mei and Auriault 1991; Firdaouss et al. 1997; Wodie and Levy 1991), with theoretical results for periodic porous media. In particular, Firdaouss et al. (1997) have shown that $\mathbf{f}^{(1)}$ must be zero for periodic porous media which verify the reversibility assumption

$$\mathbf{g}_{\beta}(-\boldsymbol{\lambda}, v) = -\mathbf{g}_{\beta}(\boldsymbol{\lambda}, v) + O\left(\delta^2\right). \tag{22}$$

For example, a square array of cylinders verifies exactly the reversibility assumption, due to symmetry properties. It has further been shown (Mei and Auriault 1991; Wodie and Levy 1991) that $F_{\parallel}^{(1)} = 0$ in periodic porous media, while the orthogonal term $F_{\perp}^{(1)}$ is a priori nonzero. This yields a *partial* cubic regime in the general case, or the cubic regime in the specific case of porous media for which $F_{\perp}$ vanishes due to characteristics of the microstucture. Such media are defined as *isotropic*, but it is likely that a zero $F_{\perp}$ requires a *disordered* microstructure, or a symmetry condition. Indeed ordered porous media may be isotropic with respect to the permeability ($\mathbf{K}_{\mathrm{D}} = K_{\lambda}\mathbf{I}$), while the $F_{\perp}$ term is nonzero (e.g., Koch and Ladd 1997).

Mei and Auriault (1991), Firdaouss et al. (1997) and Wodie and Levy (1991), asymptotic expansions are performed on both the Reynolds number Re_{C}, and the ratio of microscopic and macroscopic scales

$$\epsilon_{\mathrm{l}} = \frac{\ell_{\beta}}{L_{\mathrm{v}}}, \tag{23}$$

where for *technical* reasons intrinsic to the asymptotic method, the value of Re_{C} is related to the value of ϵ_{l}. Although there are cases for which this relation is justified, there is no *physical* reasons for this relation in the general case, as ϵ_{l} and Re_{C} are *a priori* independent parameters. In particular, the assumption $\epsilon_{\mathrm{l}} \ll 1$ does not require Re_{C} to be small. Even for turbulent flows where $Re_{\mathrm{C}} \gg 1$, the length scales separation assumption holds ($\epsilon_{\mathrm{l}} \ll 1$) in homogeneous porous media (Jin et al. 2015). Moreover, a creeping flow may encounter strong shear, yielding $Re_{\mathrm{C}} \ll 1$ while $\epsilon_{\mathrm{l}} \sim 1$.

Our approach recovers all these theoretical results from the literature. We show that $F_{\parallel}^{(1)} = 0$ (see "Appendix C") for any periodic porous medium. For media that satisfy the reversibility assumption, $F_{\perp}^{(1)} = 0$ is required for our AGF to be consistent. In the framework of volume averaging, we have derived the closure problem before carrying out the perturbation analysis in Re_{C}, keeping ϵ_{l} and Re_{C} independent. The form of our closure problem is further validated by DNS in Sect. 3.2.1.

2.3 Inertial Sensitivity Parameter

We use the closure problem (Eq. 64) to develop a dimensionless number that characterizes the Darcy/non-Darcy transition. To do so, we use Eqs. 5 and 14 and rewrite the first equation in System 64 as

$$\underbrace{\frac{\ell v}{\nu_{\beta}}\mathbf{v}^{*}\cdot\nabla^{*}\mathbf{v}^{*}}_{\text{(I)}} = -\nabla^{*}p^{*} + \nabla^{*2}\mathbf{v}^{*} + \underbrace{\epsilon_{\beta}\ell^{2}\left(\mathbf{K}_{\mathrm{D}}^{-1}\cdot\boldsymbol{\lambda} + \mathbf{f}\right)}_{\text{(II)}}. \tag{24}$$

In the creeping flow regime, term (I) in Eq. 24 is negligible and term (II) is the only source term. As the flow rate increases, $\mathbf{f}$ becomes important via the increasing importance of term (I). We thus consider the ratio of the orders of magnitude of terms (I) and (II). As term (II) is of order $\epsilon_{\beta}\ell^{2}K_{\lambda}^{-1}$ at the Darcy/non-Darcy transition, we have

$$\frac{\text{(I)}}{\text{(II)}} \simeq \frac{\ell v}{\nu_{\beta}}\frac{\zeta\left(\mathbf{v}^{*}\cdot\nabla^{*}\mathbf{v}^{*}\right)}{\epsilon_{\beta}\ell^{2}K_{\lambda}^{-1}}, \tag{25}$$

where the symbol ζ defines a norm for the field $\mathbf{v}^{*}\cdot\nabla^{*}\mathbf{v}^{*}$. ζ is essential in the evaluation of the order of magnitude of term (I). Any choice for ζ is acceptable, depending on the goal of

the study. A choice of ζ is proposed in Sect. 3, where our goal is to find the proper Reynolds number to assess the validity of Darcy's law for a variety of porous media.

We now wish to eliminate ℓ from Eq. 24 and start from the consideration that, at steady state, the total rate of work of the pressure gradient balances the total internal viscous dissipation over the REV

$$\int_{\mathscr{V}_\beta} \mathbf{v}_\beta \cdot \left(-\mathbf{g}_\beta\right) \mathrm{d}V = \int_{\mathscr{V}_\beta} \mu_\beta \nabla \mathbf{v}_\beta :^{\mathrm{T}} \nabla \mathbf{v}_\beta \, \mathrm{d}V. \tag{26}$$

We integrate a second time over $\mathscr{V}_\beta$ and recall Eq. 50 to obtain

$$-\left\langle \mathbf{v}_\beta \right\rangle^\beta \cdot \mathbf{g}_\beta = \mu_\beta \left\langle \nabla \mathbf{v}_\beta :^{\mathrm{T}} \nabla \mathbf{v}_\beta \right\rangle^\beta. \tag{27}$$

Rewriting the left-hand-side with definition 5 yields

$$\left\langle \nabla \mathbf{v}_\beta :^{\mathrm{T}} \nabla \mathbf{v}_\beta \right\rangle^\beta = \boldsymbol{\lambda} \cdot \epsilon_\beta \left(\mathbf{K}_{\mathrm{D}}^{-1} \cdot \boldsymbol{\lambda} + \mathbf{f} \right) \simeq \boldsymbol{\lambda} \cdot \epsilon_\beta \mathbf{K}_{\mathrm{D}}^{-1} \cdot \boldsymbol{\lambda}, \tag{28}$$

at the Darcy/non-Darcy transition. Using the change of variables of Eq. 57, we can write

$$\ell^2 \boldsymbol{\lambda} \cdot \epsilon_\beta \mathbf{K}_{\mathrm{D}}^{-1} \cdot \boldsymbol{\lambda} = \left\langle \nabla^* \mathbf{v}^* :^{\mathrm{T}} \nabla^* \mathbf{v}^* \right\rangle^\beta. \tag{29}$$

This gives an expression for ℓ, as

$$\ell = \sqrt{\frac{\left\langle \nabla^* \mathbf{v}^* :^{\mathrm{T}} \nabla^* \mathbf{v}^* \right\rangle^\beta}{\boldsymbol{\lambda} \cdot \epsilon_\beta \mathbf{K}_{\mathrm{D}}^{-1} \cdot \boldsymbol{\lambda}}}, \tag{30}$$

which we use in Eq. 25

$$\frac{(\mathrm{I})}{(\mathrm{II})} \simeq \frac{v}{\nu_\beta} \sqrt{\frac{K_\lambda}{\epsilon_\beta}} \frac{\zeta \left(\mathbf{v}^* \cdot \nabla^* \mathbf{v}^* \right)}{\sqrt{\left\langle \nabla^* \mathbf{v}^* :^{\mathrm{T}} \nabla^* \mathbf{v}^* \right\rangle^\beta}} \sqrt{\frac{\boldsymbol{\lambda} \cdot \mathbf{K}_{\mathrm{D}}^{-1} \cdot \boldsymbol{\lambda}}{K_\lambda^{-1}}}. \tag{31}$$

We approximate $\mathbf{v}^*$ by $\mathbf{v}_0^*$, a zero-order approximation in terms of δ (see Eq. 19), and obtain

$$\frac{(\mathrm{I})}{(\mathrm{II})} \simeq \frac{v}{\nu_\beta} \sqrt{\frac{K_\lambda}{\epsilon_\beta}} \frac{\zeta \left(\mathbf{v}_0^* \cdot \nabla^* \mathbf{v}_0^* \right)}{\sqrt{\left\langle \nabla^* \mathbf{v}_0^* :^{\mathrm{T}} \nabla^* \mathbf{v}_0^* \right\rangle^\beta}} \sqrt{\frac{\boldsymbol{\lambda} \cdot \mathbf{K}_{\mathrm{D}}^{-1} \cdot \boldsymbol{\lambda}}{K_\lambda^{-1}}}. \tag{32}$$

We now define Re_{C} as

$$Re_{\mathrm{C}} = \frac{v}{\nu_\beta} \sqrt{\frac{K_\lambda}{\epsilon_\beta}} C_\lambda, \tag{33}$$

with the inertial sensitivity, C_λ, defined as

$$C_\lambda = \frac{\zeta \left(\mathbf{v}_0^* \cdot \nabla^* \mathbf{v}_0^* \right)}{\sqrt{\left\langle \nabla^* \mathbf{v}_0^* :^{\mathrm{T}} \nabla^* \mathbf{v}_0^* \right\rangle^\beta}} \sqrt{\frac{\boldsymbol{\lambda} \cdot \mathbf{K}_{\mathrm{D}}^{-1} \cdot \boldsymbol{\lambda}}{K_\lambda^{-1}}}, \tag{34}$$

such that by construction

$$Re_{\mathrm{C}} \simeq \frac{(\mathrm{I})}{(\mathrm{II})}. \tag{35}$$

The length scale ℓ therefore corresponds to

$$\ell = \sqrt{\frac{K_\lambda}{\epsilon_\beta}} C_\lambda. \tag{36}$$

The distribution pattern of the advective term $\mathbf{v}_0^* \cdot \nabla^* \mathbf{v}_0^*$ is closely related to the microstructure and the flow direction, as shown in Fig. 5, Sect. 3.2.2. The effect of inertia on Darcy's law is driven by the shape of the microstructure, and the topological parameter C_λ measures the ability of inertia to affect Darcy's law. The inertial sensitivity C_λ is specific to both the porous medium and the flow direction $\boldsymbol{\lambda}$. We can distinguish among different cases:

- $C_\lambda \simeq 1$: $\sqrt{K_\lambda/\epsilon_\beta}$ is the proper length scale to measure the effects of inertia.
- $C_\lambda \ll 1$: $Re_\mathrm{k} = 1$ does not capture the inertial transition, as illustrated by the limit case of cylindrical pores. In this case, C_λ identically vanishes as streamlines are orthogonal to velocity gradients. Therefore, Darcy's law is correct for any Re_k in the laminar regime and breaks down only when transition to unsteady flow occurs (Skjetne and Auriault 1999).
- $C_\lambda \gg 1$: This situation is opposite to the previous one. Effects of inertia impact the macroscale Darcy's law early, while $Re_\mathrm{k} \ll 1$ still holds. There are no obvious examples of geometry for this case, but it is more likely that tortuous geometries generate large values of C_λ (see later Table 1).

This classification resolves the issue encountered with certain porous media for which $Re_\mathrm{k} \ll 1$ is not the correct order of magnitude to assess the validity of Darcy's law. The relevance of Re_C is further assessed in Sect. 3.2.2 by the interpretation of numerical experiments over a variety of porous structures.

3 Numerical Results

We test the AGF and validate the relevance of Re_C in describing the inertial transition on model and realistic porous media with various microstructures (Fig. 2). We consider

- Two-dimensional arrangements of cylinders,
- Two-dimensional convergent-divergent unit cells of equal throat size,
- Two- and three-dimensional geometries exhibiting complex, realistic geometrical features, obtained by x-ray tomography imaging of a sandstone.

The acronyms of all studied geometries are provided in Table 1.

3.1 Method

Flow simulations are carried out with the C++ toolbox Open∇FOAM® , which allows for the development of numerical solvers, and comes up with pre- and post-processing utilities for computational fluid dynamics (CFD). Open∇FOAM® is released as free and open-source software, and this allows the user to customize the source code in order to implement her/his own problem. This aspect of Open∇FOAM® is crucial, because in order to compute the coefficients of the asymptotic form of $F_\parallel$, we need to solve Stokes problems obtained in "Appendix B" with specific source terms. We use a classical finite-volume discretization method. For each cell of the mesh, an integral form of the equations to solve is obtained by integrating the momentum- and mass- conservation law over the volume of the cell. The

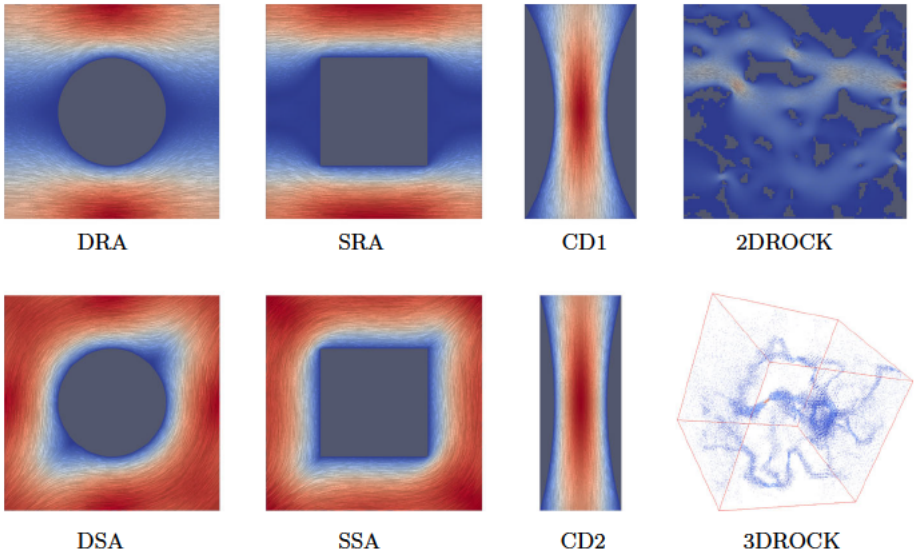

Fig. 2 Normalized fields of velocity magnitude for Stokes flows through the considered porous media. Small (large) values correspond to blue (red) area. We refer to Table 1 for the meaning of the acronyms that we use to refer to each porous medium

Table 1 Computed values of C_λ and $F_\parallel^{(2)}$ for each porous media

Short-cut	C_λ	$F_\parallel^{(2)}$	medium
3DROCK	176	$1.07 \times 10^{+03}$	Three-dimensional rock
2DROCK	5.77	3.92×10^{-01}	Two-dimensional rock
DSA	0.62	2.84×10^{-02}	Disks in staggered arrangement
DRA	0.49	8.46×10^{-03}	Disks in regular arrangement
SSA	0.77	3.77×10^{-02}	Squares in staggered arrangement
SRA	0.36	4.43×10^{-03}	Squares in regular arrangement
CD1	0.19	1.08×10^{-03}	Convergent-divergent 1
CD2	0.10	3.00×10^{-04}	Convergent-divergent 2

The acronym and full name of each porous medium are indicated as well

Gauss theorem is then applied to write the volume integrals as surface integrals, which involve field and gradient evaluation on cell faces. The evaluation of different quantities on cell faces is performed by linear interpolation between cell centers, or by use of a finite difference scheme for the gradients.

For periodic geometries, imposition of periodic boundary conditions is trivial. For the 3DROCK case, while periodic conditions are imposed on the inlet and outlet faces by adding a thin layer of fluid, symmetry conditions are imposed on other faces. One should notice that this is equivalent to symmetrizing the geometry and imposing periodic conditions. Symmetry conditions are also imposed on each side of the 2DROCK case. As the order of the discretization method is relatively low, and because we need a relatively high accuracy in our simulations, the number of mesh points to achieve mesh independence can be very large. We

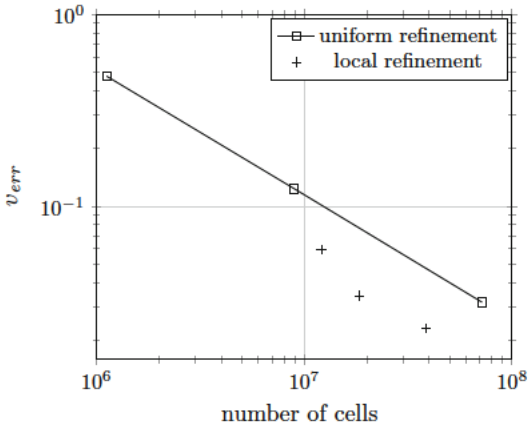

Fig. 3 Mesh convergence for the 3DROCK geometry. The local refinement strategy accelerates the convergence to mesh independence compared to the uniform refinement strategy

must adopt the proper method according to the geometry of interest. Since we are interested in the value of the macroscopic parameter $F_{\|}$, we only use a macroscopic convergence criterion to assess mesh independence. For a given value of the pressure gradient, we compute the relative error on v between two refinement levels to evaluate the accuracy of the simulation. For 2D geometries, we use a simple uniform mesh and uniformly refine until mesh independence is achieved. Hence, the fine mesh is a uniform structured hexahedral mesh for these geometries. For the 3DROCK case, however, this simple approach would involve a too large computational cost.

Mesh independence with a uniform structured hexahedral mesh for the 3DROCK geometry is achieved with 5.73×10^8 cells. This number of cells is comparable to the number of cells used in other numerical study of the inertial deviation from Darcy's law in sandstones, see, e.g., Muljadi et al. (2016). This requires approximately 10^4cores hours to converge on the supercomputer EOS-CALMIP. This large cost in CPU time is due to the fact that the 3DROCK geometry is a 3D, tortuous geometry that contains many more pore throats and sizes than the other simple geometries studied here. Typically, the ratio of the largest pore size to the smallest pore throat is around 10 for the 3DROCK. To reduce the number of mesh points, local refinements are performed for the 3DROCK geometry. We first compute an expensive reference solution with a uniform structured hexahedral mesh. Then, a coarser mesh that gives low-accuracy results is locally refined only in regions where the value of the viscous dissipation is above a certain threshold (i.e. , regions of high velocity gradients $\nabla \mathbf{v}_\beta$). For each level of refinement, the threshold of viscous dissipation above which cells are refined is adjusted to find a compromise between the number of cells and the accuracy of the simulation. This process allows to approximate fairly well the reference solution (within the desired accuracy criterion) with only 1.8×10^7 mesh cells (Fig. 3). As a result, the local refinement process reduces the required amount of CPU time by an order of magnitude, making simulations on the 3DROCK medium tractable.

3.2 Inertial Effects

For each geometry, K_λ is first computed by carrying out Stokes flow simulations. We then solve for the Navier–Stokes equations (Eq. 13) and compute $F_{\|}$ from Eq. 16. The drag Forchheimer term $F_{\|}$ is plotted in Fig. 4 as a function of the Reynolds numbers Re_k for the porous media represented in Fig. 2.

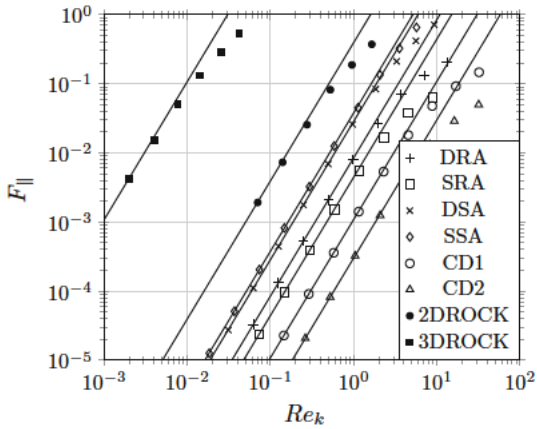

Fig. 4 Drag Forchheimer term $F_\parallel$ as function of Re_k. Data from DNS (symbols) and AGF (solid lines)

3.2.1 Asymptotic Form

To validate the developments of Sect. 2.2 and the form of the CP that is the base of our theory, we compute coefficients of the asymptotic form of $F_\parallel$ for the considered porous media. For that purpose, the derivation of the system of equations to resolve for each order i is presented in full details in "Appendix B." These developments yield

$$\mathbf{S}_i^* = -\nabla^* p_i^* + \nabla^{*2}\mathbf{v}_i^* + \epsilon_\beta \mathbf{h}_i^*, \tag{37a}$$

$$\nabla^* \cdot \mathbf{v}_i^* = 0, \tag{37b}$$

$$\mathbf{v}_i^* = 0 \text{ at } \mathscr{A}_{\beta\sigma}, \tag{37c}$$

The same numerical method as the one described above is adapted to resolve Eq. 66, with proper source terms $\mathbf{S}_i^*$. These source terms are given explicitely in "Appendix B." As explained in "Appendix B," the numerical resolution of Eq. 66 provides $F_\parallel^{(i)}$ at any order i. The numerical results for $F_\parallel^{(i)}$ are shown in Table 1. For each geometry, $F_\parallel^{(1)}$ is zero (up to the order of accuracy of the simulation) and $F_\parallel^{(2)}$ accurately matches the DNS (see Fig. 4, solid lines), therefore validating our form of CP. Furthermore, the scaling $F_\parallel \sim Re_\mathrm{C}^2$ of the weak inertia regime is universal across the samples tested. A possible expression of the Forchheimer number to capture the limit of Darcy's law is (here, $F_\perp \ll F_\parallel$)

$$F_\lambda = F_\parallel^{(2)} Re_\mathrm{k}^2, \tag{38}$$

with the inertial deviation from Darcy's law occuring at $F_\lambda = 0.1$. As shown by experiments (Forchheimer 1901; Ergun 1952; Clavier 2015), a quadratic dependence of the pressure drop on the flow rate eventually occurs, but this regime is beyond the velocity range studied here and cannot be captured by our asymptotic development.

3.2.2 Validation of Re_C

Figure 4 shows the different behaviors of $F_\parallel$ for the various media considered; notably, the 3DROCK geometry has a very early deviation from Darcy's law. This result is in agreement with the results obtained in Muljadi et al. (2016). In this article, the authors evaluate the deviation from Darcy's law on a few sample of sandstones. They find that the value of the

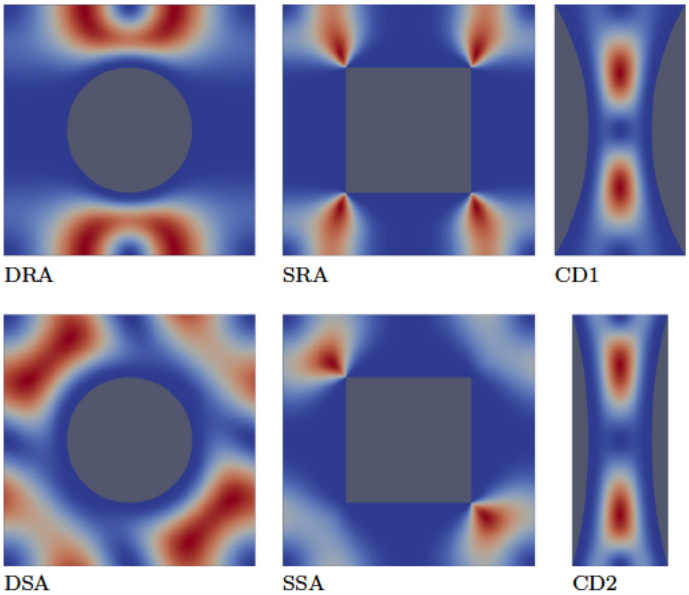

Fig. 5 Normalized fields of $||\mathbf{v}_0^* \cdot \nabla^* \mathbf{v}_0^*||$ in model porous media. Small (large) values correspond to blue (red) area

Reynolds numbers at the deviation from Darcy's law varies of several orders of magnitude, depending on the type of sandstone. Such differences cannot be captured only by a pore throat size or even by a permeability-based Reynolds numbers. This is because Reynolds numbers based only on porosity, permeability and pore size cannot differentiate geometries depending on their ability to develop advection dominated areas as the Reynolds number increases. This can be better accounted for by Re_C thanks to the inertial sensitivity C_λ. To illustrate this, we evaluate C_λ for porous media represented in Fig. 2, from Eqs. 33 and 34, recalling that C_λ depends on the advective term $\mathbf{v}_0^* \cdot \nabla^* \mathbf{v}_0^*$ (*cf.* Eq. 34).

In Fig. 5, we can visualize the normalized fields of $||\mathbf{v}_0^* \cdot \nabla^* \mathbf{v}_0^*||$ in the selected ordered porous media. The pattern is very different from a geometry to another. C_λ, via ζ, uses this signature to characterize the topology of a porous medium in terms of the distribution of the advective term within it. To do so, we propose to define ζ as a generalized mean of order n

$$\zeta\left(\mathbf{v}_0^* \cdot \nabla^* \mathbf{v}_0^*\right) = \left(\left\langle ||\mathbf{v}_0^* \cdot \nabla^* \mathbf{v}_0^*||^n \right\rangle^\beta\right)^{1/n}. \tag{39}$$

We have tested a few values of n in Eq. 39. Results are plotted in Fig. 6. For $n = 1$, while the curves collapse well for simple geometries, there is still a gap between $2D$- and $3D$ROCK geometries and the other cases. We assume that this is due to the weight given to high values of $||\mathbf{v}_0^* \cdot \nabla^* \mathbf{v}_0^*||$ in the computation of C_λ in Eq. 34. To verify this assumption, we increase the value of n, thus augmenting the weight of high values of $||\mathbf{v}_0^* \cdot \nabla^* \mathbf{v}_0^*||$ in the computation of C_λ. While the good collapse for simple geometries is conserved, the curves of $2D$- and $3D$ROCK geometries tend to collapse with the others in Fig. 6. This suggests that the effect of inertia is more localized in $2D$- and $3D$ROCK geometries than in ordered ones. The best collapse of the curves is found for $n = 4$ and values of C_λ in Table 1 refer to this n. Connecting with Fig. 4, we observe that for each geometry, the earlier the rise in $F_\parallel$, the larger the value of C_λ; this shows that the form of ζ allows C_λ to be a consistent

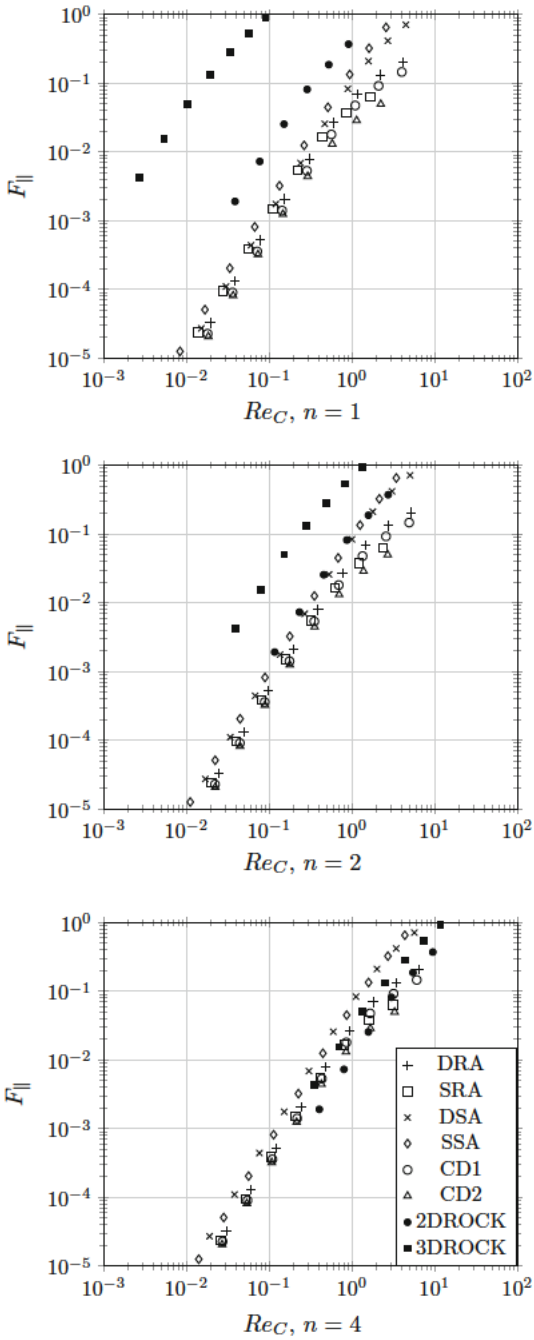

Fig. 6 *Parallel* component of the inertial correction for different definitions of Re_C. The bottom frame shows that inertial transition starts at $Re_C \sim 1$ for all model porous media when $n = 4$

indicator to predict the strength of the effects of inertia on Darcy's law. From a quantitative point of view, Re_C is a much better indicator than Re_k, as the data scatter on the bottom plot of Fig. 6 is much reduced compared to Fig. 4. This is further emphasized below in the case of anisotropic porous media.

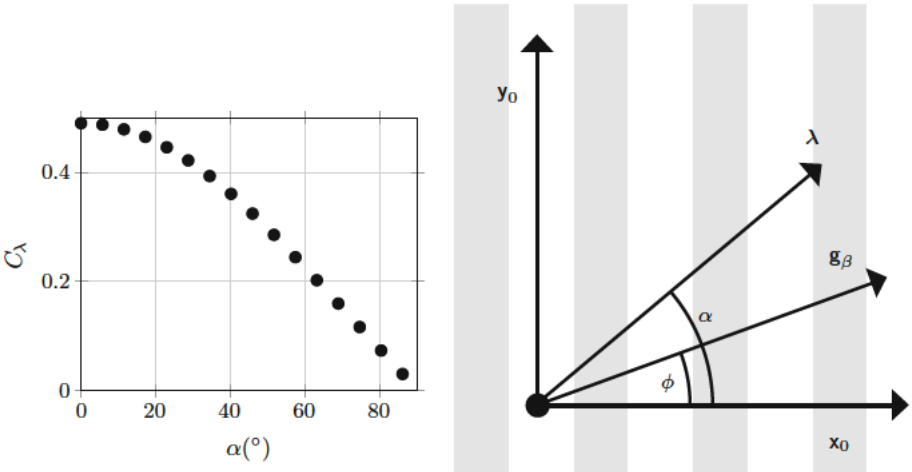

Fig. 7 C_λ as a function of α for a regular array of cylinders. $\alpha = 0$ corresponds to a flow orthogonal to the cylinders axis, ($\alpha = \pi/2, C_\lambda = 0$) corresponds to a flow parallel to the cylinders axis. Values of C_λ are computed from Eq. 34 with $n = 4$

3.3 Filtration Law for a Model Anisotropic Structure

While in the linear regime the tensorial writing of Darcy's law (Eq. 3) provides a filtration law for any flow direction, a difficult issue with inertial flows is the derivation of the filtration law in anisotropic porous media, since the characteristics of the filtration law must be determined for each direction. An expensive solution consists in building a dataset by numerical simulations or experiments, for each Reynolds number and direction of the flow (Luminari et al. 2018). Here, we propose a solution for a restricted range of Reynolds number, but at a much more affordable cost than the DNS, as it requires only a few flow simulations to give a filtration law for any direction.

We consider an orthotropic porous medium made of a regular arrangement of cylinders (Fig. 7) of porosity $\epsilon_\beta = 0.8036$. Let ϕ be the angle between the pressure gradient and the cylinders' axis. For three values of ϕ, the evolution of $F_\parallel$ as a function of Re_k and Re_C is displayed in Fig. 8. For a given ϕ, the flow direction varies with Re_C. Hence, $C_\lambda(\phi)$ is computed for the flow direction corresponding to $F_\parallel = 0.1$

$$C_\lambda(\phi) = C_\lambda\left(\boldsymbol{\lambda}\left(\phi, F_\parallel = 0.1\right)\right). \tag{40}$$

Figure 8 shows that with this definition, the curves of $F_\parallel$ and $F_\perp$ tend to collapse. We now explain how this can be used to derive a filtration law for this range of Re_C.

As $\mathbf{v}_0^*$ arises from a Stokes equation, the $\mathbf{v}_0^*$ field corresponding to a given flow direction $\boldsymbol{\lambda}$ can be obtained as

$$\mathbf{v}_0^* = \mathbf{M}_0^* \cdot \boldsymbol{\lambda}, \tag{41}$$

where $\mathbf{M}_0^*$ is solution of (see "Appendix B")

$$0 = -\nabla^* \mathbf{m}_0^* + \nabla^{*2}\mathbf{M}_0^* + \epsilon_\beta \ell^2 \mathbf{K}_\mathrm{D}^{-1}, \tag{42a}$$

$$\nabla^* \cdot \mathbf{M}_0^* = 0, \tag{42b}$$

$$\mathbf{M}_0^* = 0 \text{ at } \mathscr{A}_{\beta\sigma}. \tag{42c}$$

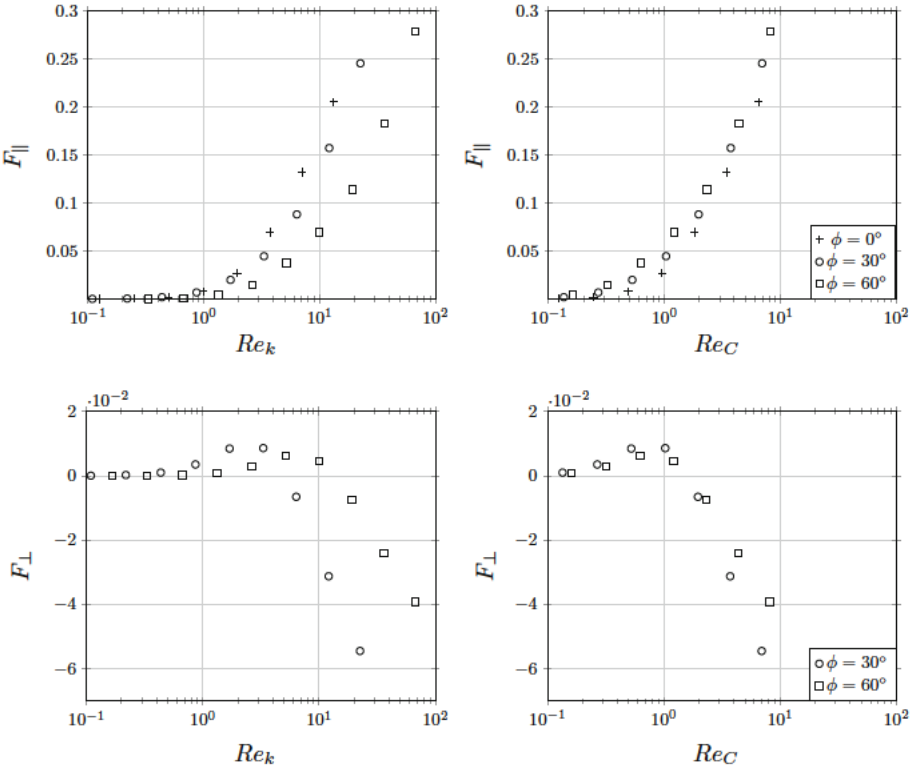

Fig. 8 $F_\parallel$ and $F_\perp$ as function of Re_k and Re_C for a regular array of cylinders. Re_C is computed from Eq. 33. Values of C_λ are provided in Fig. 7

Let ϕ be the angle between the pressure gradient and the cylinders' axis. This allows to determine C_λ for any flow direction $\boldsymbol{\lambda}$ (Fig. 7) with only three flow simulations in three independent directions of space, in order to build $\mathbf{M}_0^*$. Then, instead of building an expensive dataset, we can compute the profile of $\left(F_\parallel, F_\perp\right)$ for one value of the flow direction $\boldsymbol{\lambda}^0$, to generalize to any values of $\boldsymbol{\lambda}$. Indeed, the collapse of the curves in Fig. 8 translates into

$$\left(F_\parallel, F_\perp\right)(\boldsymbol{\lambda}, v) = \left(F_\parallel, F_\perp\right)\left(\boldsymbol{\lambda} = \boldsymbol{\lambda}^0, Re_C(\boldsymbol{\lambda}, v)\right), \tag{43}$$

which provides a profile for $F_\parallel(\phi, v)$ and $F_\perp(\phi, v)$ with a limited number of simulations. This feature is of importance in applications for which a large number of simulations is prohibited due to the large amount of computational time required.

4 Conclusion

The volume-averaging method is used to investigate the onset of inertial effects for flows in porous media. The introduction of the new Reynolds number, Re_C, captures well the Darcy/non-Darcy transition. This number contains a parameter, C_λ, which characterizes the sensitivity to inertia of a microstructure for a given flow direction, and is defined as

$$Re_{\mathrm{C}} = \frac{v\sqrt{K_\lambda/\epsilon_\beta}}{\nu_\beta} C_\lambda. \tag{44}$$

We show that this definition of Re_{C} is appropriate to measure the effect of microscopic inertia on the filtration law. Further, we find that a possible application of this new scaling is the derivation of a correction to Darcy's law for weakly inertial flows in highly anisotropic porous media, where the tensorial Darcy's law collapses.

Finally, our study focuses on the evolution of $F_\parallel$, while the examination of the orthogonal component $F_\perp$ and of the angle ω (Eq. 16) is left for future work. Anisotropic, ordered, three-dimensional microstructures are expected to generate varying features of $F_\perp$ and ω with increasing Re_{C}; such features are the object of current research efforts.

Acknowledgements The authors would like to thank the IDEX Foundation of the University of Toulouse for the financial support granted to AB under the project "Attractivity Chairs." This work was granted access to the HPC resources of CALMIP supercomputing center under the allocation 2016-p1540.

A Derivation of the Filtration Law

In this section, we give some technical details of the derivation of the filtration law by the volume-averaging method.

A.1 Upscaling via Volume Averaging

We volume-average Eq. 13 in order to obtain a representation at the macroscopic scale. To do so, we first recall a few fundamental steps. Let ψ be a generic field, and γ_β be the β-phase indicator. We define the averaging volume $\mathscr{V}(\mathbf{x})$ of characteristic length ℓ_0, whose centroid is located in $\mathbf{x}$ (which can be in any of the two phases, see Fig. 1). The intrinsic average of ψ at point $\mathbf{x}$ is defined in a general way as

$$\langle\psi\rangle^\beta|_{\mathbf{x}} = \int_{\mathbb{R}^3} m(\mathbf{r}-\mathbf{x})\,\gamma_\beta(\mathbf{r})\,\psi(\mathbf{r})\,\mathrm{d}V(\mathbf{r}), \tag{45}$$

where $\mathbf{r} = \mathbf{x} + \mathbf{y}_\beta$. This definition of the intrinsic average $\langle\psi\rangle^\beta|_{\mathbf{x}}$ allows to choose m so that the resulting intrinsic average is suitable to the porous medium that we volume-average (Quintard and Whitaker 1994a; Davit and Quintard 2017). m is a kernel normalized so that

$$\int_{\mathbb{R}^3} m(\mathbf{r})\,\gamma_\beta(\mathbf{r})\,\mathrm{d}V(\mathbf{r}) = 1. \tag{46}$$

In the following we drop the $|_{\mathbf{x}}$ subscript when there is no ambiguity regarding the point where the average is evaluated.

The volume-averaging method uses a perturbation decomposition of the fields. Each field ψ is decomposed as the sum of an average field, $\langle\psi\rangle^\beta$, and a *spatial deviation*, $\tilde{\psi}$, so that

$$\psi = \langle\psi\rangle^\beta + \tilde{\psi}, \tag{47}$$

with the underlying idea that

$$||\nabla\langle\psi\rangle^\beta|| \ll ||\nabla\tilde{\psi}||. \tag{48}$$

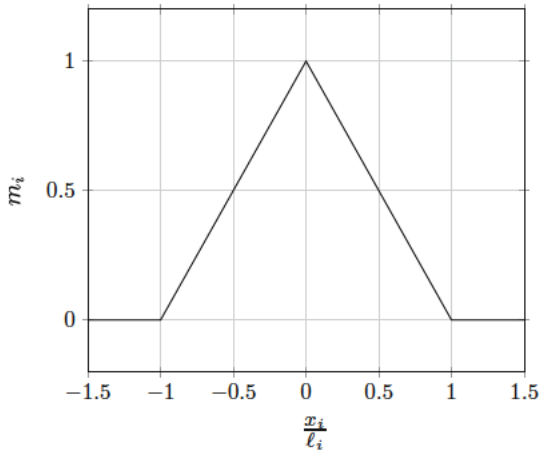

Fig. 9 One-dimensional cellular filter, following the concept of *double average* introduced in Quintard and Whitaker (1994a). ℓ_i is the dimension of the REV in the ith direction. Notice that the support of the cellular filter is twice as large as the dimension of the REV

The triangular *cellular filter* drawn in Fig. 9 is a good choice for m [concept of *double average* introduced in Quintard and Whitaker (1994a)]. In 3D, $m(\mathbf{x})$ takes the form

$$m(\mathbf{x}) = \prod_{i=1,3} m_i(x_i). \tag{49}$$

Let $\mathscr{V}_\beta(\mathbf{x})$ be the domain filled with the fluid phase inside the averaging volume $\mathscr{V}(\mathbf{x})$ and let V_β be the measure of $\mathscr{V}_\beta(\mathbf{x})$. It is useful to note that the cellular filter is such that

$$\int_{\mathbb{R}^n} m(\mathbf{r}-\mathbf{x})\,\psi(\mathbf{r})\,\mathrm{d}V(\mathbf{r}) = \frac{1}{V_\beta}\int_{\mathscr{V}_\beta(\mathbf{x})}\left(\frac{1}{V_\beta}\int_{\mathscr{V}_\beta(\mathbf{y})}\psi(\mathbf{r})\,\mathrm{d}V(\mathbf{r})\right)\mathrm{d}V(\mathbf{y}). \tag{50}$$

In particular the average of a periodic field is such as

$$\int_{\mathbb{R}^n} m(\mathbf{r}-\mathbf{x})\,\psi(\mathbf{r})\,\mathrm{d}(\mathbf{r}) = \frac{1}{V_\beta}\int_{\mathscr{V}_\beta(\mathbf{x})}\psi(\mathbf{r})\,\mathrm{d}V(\mathbf{r}). \tag{51}$$

Since our porous medium is homogeneous and periodic, the kernel m defined by Eq. 49 ensures differentiable average pressure and velocity fields, and volume-averaging Eq. 13 yields a local macroscopic equation. The order upon which the macroscopic equation can be stated depends on the regularity of m. Here m is only C^0; hence, average quantities are only C^1 and Taylor expansions of average quantities are truncated with a second-order error (Quintard and Whitaker 1994a; Davit and Quintard 2017). We obtain

$$\nabla\langle p_\beta\rangle^\beta - \rho_\beta \mathbf{s}_\beta = \int_{\mathbb{R}^n} m(\mathbf{r}-\mathbf{x})\,\delta_{\beta\sigma}(\mathbf{r})\,\mathbf{n}_{\beta\sigma}\cdot\left(-\mathbf{I}\tilde{p}_\beta + \mu_\beta\nabla\tilde{\mathbf{v}}_\beta\right)\mathrm{d}V(\mathbf{r}) + O\left(\frac{\ell_0}{L_\mathrm{v}}\right)^2, \tag{52}$$

under the assumption that

$$\ell_0 \ll L_\mathrm{v}, \tag{53}$$

where L_v is a characteristic macroscopic length.

We can now give a precise definition of the macroscopic pressure drop $\mathbf{g}_\beta$ as

$$\mathbf{g}_\beta = \nabla\langle p_\beta\rangle^\beta - \rho_\beta \mathbf{s}_\beta. \tag{54}$$

In Eq. 52, we neglected macroscopic advection and diffusion terms, provided separation of microscopic and macroscopic length scales of the velocity field (Whitaker 1996)

$$||\nabla \left\langle \mathbf{v}_\beta \right\rangle^\beta || \ll ||\nabla \tilde{\mathbf{v}}_\beta||. \tag{55}$$

This assumption is reasonable in homogeneous porous media, far from macroscopic boundaries. Thus, for example, the region under study should not lie in a strong shear layer, nor near a wall or a crack.

A.2 The Closure Problem for Spatial Deviations

Equation 52 is a form of the volume-averaged Navier–Stokes equations which needs additional equations (i.e. , a *closure*) for the surface integral term to be evaluated. To derive these equations, we first need to decompose Eq. 13 applying Eq. 47 to $\mathbf{v}_\beta$ and p_β. By virtue of Eq. 55, we neglect gradients of macroscopic velocities against those of the microscopic velocities in the momentum transport equation and obtain

$$\left(\left\langle \mathbf{v}_\beta \right\rangle^\beta + \tilde{\mathbf{v}}_\beta\right) \cdot \nabla \tilde{\mathbf{v}}_\beta = -\tfrac{1}{\rho_\beta} \nabla \tilde{p}_\beta + \nu_\beta \nabla^2 \tilde{\mathbf{v}}_\beta - \tfrac{\mathbf{g}_\beta}{\rho_\beta}, \tag{56a}$$

$$\nabla \cdot \tilde{\mathbf{v}}_\beta = 0, \tag{56b}$$

$$\tilde{\mathbf{v}}_\beta = -\left\langle \mathbf{v}_\beta \right\rangle^\beta \text{ on } \mathscr{A}_{\beta\sigma}. \tag{56c}$$

At this stage, it is common to introduce a tensorial relation between space deviations and the intrinsic average of the velocity $\left\langle \mathbf{v}_\beta \right\rangle^\beta$ (Whitaker 1996). This mapping is adapted to the linear, creeping flow regime, as it expresses the fact that the microscopic flow field is a linear combination of the flow in three independent directions of space. Clearly this is not adapted here due to the nonlinear term in Eq. 56. We therefore drop the linear closure relationship of Whitaker (1996) and keep working with the deviation fields. We introduce the modified dimensionless perturbations $\mathbf{v}^*$ and p^* defined as

$$\mathbf{v}^* = \frac{\tilde{\mathbf{v}}_\beta}{v} + \boldsymbol{\lambda}, \;\; p^* = \ell \frac{\tilde{p}_\beta}{\mu_\beta v}, \tag{57}$$

with ℓ as yet undefined. Under such circumstances

$$\nabla \tilde{\mathbf{v}}_\beta = v \left(\nabla \mathbf{v}^* + \frac{\nabla v}{v} \mathbf{v}^* - \frac{\nabla \left\langle \mathbf{v}_\beta \right\rangle^\beta}{v} \right), \;\; \nabla \tilde{p}_\beta = v \frac{\mu_\beta}{\ell} \left(\nabla p^* + p^* \frac{\nabla v}{v} \right). \tag{58}$$

We inject Eqs. 57 and 58 into Eq. 56. Under the assumption given by Eq. 55 we obtain

$$\frac{\ell}{\nu_\beta} v|_{\mathbf{x}+\mathbf{y}_\beta} \left(\mathbf{v}^* \cdot \nabla^* \mathbf{v}^* \right) = -\nabla^* p^* + \nabla^{*2} \mathbf{v}^* + \epsilon_\beta \mathbf{h}^*, \tag{59}$$

where

$$\mathbf{h}^* = -\frac{\ell}{\epsilon_\beta \mathsf{V}_\beta} \int_{\mathscr{A}_{\beta\sigma}} \mathbf{n}_{\beta\sigma} \cdot \left(-\mathbf{I} p^* + \nabla^* \mathbf{v}^* \right) dA, \tag{60a}$$

$$\nabla^* = \ell \nabla. \tag{60b}$$

The weighting function m does not appear in the surface integral, due to the spatially periodic model that we introduce later for the closure variables $\mathbf{v}^*$ and p^* (Quintard and Whitaker

1994b). Compared to the linear case, a non-local term remains in Eq. 59. As we intend to solve for $\mathbf{v}^*$ and p^* on a REV of characteristic size ℓ_0, we linearize

$$v|_{\mathbf{x}+\mathbf{y}_\beta} = v\left[1 + \frac{\mathbf{y}_\beta}{\ell}\cdot\frac{\nabla^* v}{v} + O\left(\frac{\ell_0}{L_\mathrm{v}}\right)^2\right]. \tag{61}$$

We also have that

$$\left\langle \mathbf{v}_\beta \right\rangle^\beta = \left\langle \mathbf{v}^* v \right\rangle^\beta \tag{62a}$$

$$= v\left[\left\langle \mathbf{v}^* \right\rangle^\beta + \left\langle \mathbf{v}^* \frac{\mathbf{y}_\beta}{\ell}\right\rangle^\beta \cdot \frac{\nabla^* v}{v} + O\left(\frac{\ell_0}{L_\mathrm{v}}\right)^2\right], \tag{62b}$$

hence

$$\left\langle \mathbf{v}^* \right\rangle^\beta = \boldsymbol{\lambda} - \left\langle \mathbf{v}^* \frac{\mathbf{y}_\beta}{\ell}\right\rangle^\beta \cdot \frac{\nabla^* v}{v} + O\left(\frac{\ell_0}{L_\mathrm{v}}\right)^2. \tag{63}$$

We define the REV as the unit cell of our periodic porous medium. This is consistent with the flow regimes considered. In many systems there may be transport processes with characteristic length scales much larger than the unit cell of the microstructure, as argued in, e.g. , Jin et al. (2015), Agnaou et al. (2016) and de Carvalho et al. (2017). In such cases, one cannot reduce the REV to the unit cell of the porous medium and would need to determine an actual REV size for the flow process to be represented adequately.

We add *periodic conditions* at the boundaries of the REV since source terms of the problem are periodic themselves. By virtue of Eq. 53, $\frac{\nabla^* v}{v}$ terms are negligible. We therefore determine the closure variables $\mathbf{v}^*$, p^* through the approximate system

$$\frac{\ell v}{\nu_\beta}\left(\mathbf{v}^*\cdot\nabla^*\mathbf{v}^*\right) = -\nabla^* p^* + \nabla^{*2}\mathbf{v}^* + \epsilon_\beta \mathbf{h}^*, \tag{64a}$$

$$\nabla^*\cdot\mathbf{v}^* = 0, \tag{64b}$$

$$\mathbf{v}^* = 0 \text{ at } \mathscr{A}_{\beta\sigma}, \tag{64c}$$

$$\left\langle \mathbf{v}^* \right\rangle^\beta = \boldsymbol{\lambda}. \tag{64d}$$

Here it should be clear that the surface integral in Eq. 52 is well approximated by $\mathbf{h}^* v$ issued from Eq. 64, only if length scale assumptions stated by Eqs. 53 and 55 are acceptable. The filtration law is then given from Eq. 52 by

$$\frac{\ell^2}{\mu_\beta}\mathbf{g}_\beta\left(\boldsymbol{\lambda}, \delta\right) = -\mathbf{h}^* v. \tag{65}$$

Depending on v, the equation above gives the macroscopic pressure drop for a steady inertial flow in the $\boldsymbol{\lambda}$ direction.

B The Asymptotic Generalized Forchheimer Equation

We inject the expansion Eq. 19 into Eq. 64 to derive the asymptotic generalized Forchheimer equation (AGF). Order $i \geq 0$ corresponds to

$$\mathbf{S}_i^* = -\nabla^* p_i^* + \nabla^{*2}\mathbf{v}_i^* + \epsilon_\beta \mathbf{h}_i^*, \tag{66a}$$

$$\nabla^*\cdot\mathbf{v}_i^* = 0, \tag{66b}$$

$$\mathbf{v}_i^* = 0 \text{ at } \mathscr{A}_{\beta\sigma}, \tag{66c}$$

with

$$\mathbf{S}_0^* = 0, \tag{67a}$$

$$\mathbf{S}_1^* = \mathbf{v}_0^* \cdot \nabla^* \mathbf{v}_0^*, \tag{67b}$$

$$\mathbf{S}_i^* = \sum_{k+p=i-1} \left(\mathbf{v}_\mathrm{k}^* \cdot \nabla^* \mathbf{v}_p^* + \mathbf{v}_p^* \cdot \nabla^* \mathbf{v}_\mathrm{k}^* \right), \forall i \geqslant 2, \tag{67c}$$

and

$$\mathbf{h}_i^* = -\frac{\ell}{\epsilon_\beta \mathsf{V}_\beta} \int_{\mathscr{A}_{\beta\sigma}} \mathbf{n}_{\beta\sigma} \cdot \left(-\mathbf{I} p_i^* + \nabla^* \mathbf{v}_i^* \right) \mathrm{d}A. \tag{68}$$

To solve System 66 we proceed with this change of variables

$$\mathbf{v}_i^* = \mathbf{v}_{i0}^* + \mathbf{B}_0^* \cdot \mathbf{h}_i^*, \tag{69a}$$

$$p_i^* = p_{i0}^* + \mathbf{b}_0^* \cdot \mathbf{h}_i^*, \tag{69b}$$

with

$$0 = -\nabla^* \mathbf{b}_0^* + \nabla^{*2} \mathbf{B}_0^* + \epsilon_\beta \mathbf{I}, \tag{70a}$$

$$\nabla^* \cdot \mathbf{B}_0^* = 0, \tag{70b}$$

$$\mathbf{B}_0^* = 0 \text{ at } \mathscr{A}_{\beta\sigma}, \tag{70c}$$

and

$$\mathbf{S}_i^* = -\nabla^* p_{i0}^* + \nabla^{*2} \mathbf{v}_{i0}^*, \tag{71a}$$

$$\nabla \cdot \mathbf{v}_{i0}^* = 0, \tag{71b}$$

$$\mathbf{v}_{i0}^* = 0 \text{ at } \mathscr{A}_{\beta\sigma}. \tag{71c}$$

From Eq. 63 we have $\langle \mathbf{v}^* \rangle^\beta = \boldsymbol{\lambda}$. Hence, the coefficients of expansion in Eq. 19 verify

$$\left\langle \mathbf{v}_0^* \right\rangle^\beta = \boldsymbol{\lambda}, \tag{72a}$$

$$\left\langle \mathbf{v}_i^* \right\rangle^\beta = 0, \forall i \geq 1. \tag{72b}$$

Taking the average of order 0 in Eq. 69, we obtain

$$\boldsymbol{\lambda} = \left\langle \mathbf{v}_{00}^* \right\rangle^\beta + \left\langle \mathbf{B}_0^* \right\rangle^\beta \cdot \mathbf{h}_0^*. \tag{73}$$

Clearly, $\mathbf{v}_{00}^*$ and p_{00}^* are both zero, and Eq. 14 at order 0 reads

$$\mathbf{g}_\beta = -\frac{\mu_\beta}{\ell^2} \left(\left\langle \mathbf{B}_0^* \right\rangle^\beta \right)^{-1} \cdot \boldsymbol{\lambda} v = -\frac{\mu_\beta}{\ell^2} \left(\left\langle \mathbf{B}_0^* \right\rangle^\beta \right)^{-1} \cdot \left\langle \mathbf{v}_\beta \right\rangle^\beta, \tag{74}$$

which is the well-known (Darcy 1856; Whitaker 1999) Darcy's law (Eq. 3). The Darcy permeability tensor, $\mathbf{K}_\mathrm{D}$, can be identified as

$$\mathbf{K}_\mathrm{D} = \epsilon_\beta \ell^2 \left\langle \mathbf{B}_0^* \right\rangle^\beta. \tag{75}$$

Darcy's law is a zero-order approximation with regard to our perturbation analysis in δ. As the flow rate increases, inertia effects at the pore scale become increasingly important. The system goes beyond the creeping flow regime and deviates from Darcy's law.

The average of Eq. 69 gives

$$\left\langle \mathbf{v}_i^* \right\rangle^\beta = \left\langle \mathbf{v}_{i0}^* \right\rangle^\beta + \left\langle \mathbf{B}_0^* \right\rangle^\beta \cdot \mathbf{h}_i^*, \forall i \geq 1. \tag{76}$$

Recalling Eqs. 72 and 75 we obtain

$$\mathbf{h}_i^* = -\epsilon_\beta \ell^2 \mathbf{K}_\mathrm{D}^{-1} \cdot \left\langle \mathbf{v}_{i0}^* \right\rangle^\beta, \forall i \geq 1. \tag{77}$$

Hence, Eq. 14 at order $N \geq 1$ is (AGF)

$$\mathbf{g}_\beta = -\epsilon_\beta \mu_\beta \mathbf{K}_\mathrm{D}^{-1} \cdot \left(\boldsymbol{\lambda} - \sum_{i \geq 1}^{N} \left\langle \mathbf{v}_{i0}^* \right\rangle^\beta \delta^i \right) v. \tag{78}$$

C The Cubic Regime

Eq. 78 at order one gives ($\mathbf{K}_\mathrm{D}$ is symmetric[3])

$$\frac{1}{\mu_\beta} \mathbf{g}_\beta = -\epsilon_\beta v \left(\underbrace{\mathbf{K}_D^{-1} \cdot \boldsymbol{\lambda}}_{\text{Darcy term}} - \underbrace{\left\langle \mathbf{v}_{10}^* \right\rangle^\beta \cdot \mathbf{K}_\mathrm{D}^{-1} \delta}_{\text{first-order correction}} + O\left(\delta^2\right) \right). \tag{79}$$

We note that $\mathbf{v}_0^*$, $\mathbf{v}_{10}^*$, $\mathbf{B}_0^*$ verify a no-slip condition on $\mathscr{A}_{\beta\sigma}$ and periodic boundary conditions over the REV. $\mathbf{b}_0^*$ verifies periodic boundary conditions over the REV. We start by contracting Eq. 70 with $\mathbf{v}_{10}^*$

$$0 = -\mathbf{v}_{10}^* \cdot \nabla^* \mathbf{b}_0^* + \mathbf{v}_{10}^* \cdot \nabla^{*2} \mathbf{B}_0^* + \epsilon_\beta \mathbf{v}_{10}^*. \tag{80}$$

As $\mathbf{v}_{10}^*$ is divergence free, we can rewrite the first term as a divergence

$$\mathbf{v}_{10}^* \cdot \nabla^* \mathbf{b}_0^* = \nabla^* \cdot \left(\mathbf{v}_{10}^* \mathbf{b}_0^* \right). \tag{81}$$

Also

$$\mathbf{v}_{10}^* \cdot \left(\nabla^{*2} \mathbf{B}_0^* \right) = \mathbf{v}_{10j}^* \partial_i^* \left(\partial_i^* \mathbf{B}_{0jm}^* \right) \tag{82a}$$

$$= \partial_i^* \left(\mathbf{v}_{10j}^* \partial_i^* \mathbf{B}_{0jm}^* \right) - \partial_i^* \mathbf{v}_{10j}^* \partial_i^* \mathbf{B}_{0jm}^*, \tag{82b}$$

Hence, taking the average of Eq. 80, applying Gauss theorem and using boundary conditions for $\mathbf{v}_0^*$ and $\mathbf{v}_{10}^*$ we obtain

$$\epsilon_\beta \left\langle \mathbf{v}_{10}^* \right\rangle^\beta = \left\langle {}^\mathrm{T}\nabla^* \mathbf{v}_{10}^* : \nabla^* \mathbf{B}_0^* \right\rangle^\beta. \tag{83}$$

We contract the order 1 of Eq. 71 with $\mathbf{B}_0^*$

$$\left(\mathbf{v}_0^* \cdot \nabla^* \mathbf{v}_0^* \right) \cdot \mathbf{B}_0^* = -\left(\nabla^* p_{10}^* \right) \cdot \mathbf{B}_0^* + \left(\nabla^{*2} \mathbf{v}_{10}^* \right) \cdot \mathbf{B}_0^*, \tag{84}$$

rewrite

$$\left(\nabla^* p_{10}^* \right) \cdot \mathbf{B}_0^* = \nabla^* \cdot \left(\mathbf{B}_0^* p_{10}^* \right), \tag{85a}$$

$$\left(\nabla^{*2} \mathbf{v}_{10}^* \right) \cdot \mathbf{B}_0^* = \nabla^* \cdot \left(\nabla^* \mathbf{v}_{10}^* \cdot \mathbf{B}_0^* \right) - {}^\mathrm{T}\nabla^* \mathbf{v}_{10}^* : \nabla^* \mathbf{B}_0^*, \tag{85b}$$

and take the average of Eq. 84. Applying Gauss theorem and recalling the boundary conditions for $\mathbf{v}_0^*$ and $\mathbf{v}_{10}^*$, we have

$$\left\langle \mathbf{v}_0^* \cdot \nabla^* \mathbf{v}_0^* \cdot \mathbf{B}_0^* \right\rangle^\beta = -\left\langle {}^\mathrm{T}\nabla^* \mathbf{v}_{10}^* : \nabla^* \mathbf{B}_0^* \right\rangle^\beta. \tag{86}$$

[3] One can show using Eq. 70 that $\mathbf{K}_\mathrm{D}$ is symmetric [see proof in Whitaker (1999)].

With Eq. 83 we obtain

$$\epsilon_\beta \left\langle \mathbf{v}_{10}^* \right\rangle^\beta = -\left\langle \mathbf{v}_0^* \cdot \nabla^* \mathbf{v}_0^* \cdot \mathbf{B}_0^* \right\rangle^\beta . \tag{87}$$

Let $\mathbf{v}_\mathrm{d}$ such as

$$\mathbf{v}_\mathrm{d} = \ell^2 \mathbf{B}_0^* \cdot \mathbf{K}_\mathrm{D}^{-1} \cdot \mathbf{d}, \tag{88}$$

with $\mathbf{d}$ a unit vector along a generic direction. The component along $\mathbf{d}$ of the first-order correction to Darcy's law reads

$$\epsilon_\beta \ell^2 \mathbf{f}^{(1)} \cdot \mathbf{d} = \epsilon_\beta \ell^2 \left\langle \mathbf{v}_{10}^* \right\rangle^\beta \cdot \mathbf{K}_\mathrm{D}^{-1} \cdot \mathbf{d} = -\left\langle \mathbf{v}_0^* \cdot \nabla^* \mathbf{v}_0^* \cdot \mathbf{v}_\mathrm{d} \right\rangle^\beta . \tag{89}$$

Let us rewrite the $\left\langle \mathbf{v}_0^* \cdot \nabla^* \mathbf{v}_0^* \cdot \mathbf{v}_\mathrm{d} \right\rangle^\beta$ term using

$$\mathbf{v}_0^* \cdot \nabla^* \mathbf{v}_0^* \cdot \mathbf{v}_\mathrm{d} = \mathbf{v}_0^* \cdot \nabla^* \left(\mathbf{v}_0^* \cdot \mathbf{v}_\mathrm{d} \right) - \mathbf{v}_0^* \cdot \nabla^* \mathbf{v}_\mathrm{d} \cdot \mathbf{v}_0^* \tag{90a}$$

$$= \nabla^* \cdot \left(\mathbf{v}_0^* \mathbf{v}_0^* \cdot \mathbf{v}_\mathrm{d} \right) - \mathbf{v}_0^* \cdot \nabla^* \mathbf{v}_\mathrm{d} \cdot \mathbf{v}_0^*, \tag{90b}$$

so that

$$\epsilon_\beta \ell^2 \mathbf{f}^{(1)} \cdot \mathbf{d} = -\left\langle \mathbf{v}_0^* \cdot \nabla^* \mathbf{v}_0^* \cdot \mathbf{v}_\mathrm{d} \right\rangle^\beta = \left\langle \mathbf{v}_0^* \cdot \nabla^* \mathbf{v}_\mathrm{d} \cdot \mathbf{v}_0^* \right\rangle^\beta . \tag{91}$$

This is a general equation that gives information on the component in the $\mathbf{d}$ direction of the first correction to Darcy's law.

C.1 Drag Component $F_\parallel$

The direction $\mathbf{d} = \boldsymbol{\lambda}$ corresponds to

$$\epsilon_\beta \mathbf{v}_\mathrm{d} = \mathbf{v}_0^*. \tag{92}$$

With Eq. 91 we clearly have that

$$\epsilon_\beta \mathbf{v}_\mathrm{d} = \mathbf{v}_0^* \quad \text{implies} \quad \left\langle \mathbf{v}_0^* \cdot \nabla^* \mathbf{v}_0^* \cdot \mathbf{v}_\mathrm{d} \right\rangle^\beta = 0, \tag{93}$$

which is equivalent to $F_\parallel^{(1)} = 0$ due to Eq. 89, so that in a periodic porous medium

$$\frac{1}{\mu_\beta} \boldsymbol{\lambda} \cdot \mathbf{g}_\beta \left(\boldsymbol{\lambda}, v \right) = -\epsilon_\beta v \left[\boldsymbol{\lambda} \cdot \mathbf{K}_\mathrm{D}^{-1} \cdot \boldsymbol{\lambda} + O\left(\delta^2 \right) \right], \tag{94}$$

i.e. , the first drag inertial correction to Darcy's law of our AGF is cubic in terms of the average velocity.

C.2 Orthogonal Component $F_\perp$

Let $\boldsymbol{\lambda}^\perp$ be a unit vector orthogonal to the flow direction $\boldsymbol{\lambda}$. Unfortunately, Eq. 91 does not help to prove that $F_\perp^{(1)} = 0$. We can, however, show that $F_\perp^{(1)}$ must be zero under specific assumptions on the microstructure of the porous medium.

Equation 91 gives the information that $\ell^2 \mathbf{f}^{(1)} \cdot \mathbf{d}$ is quadratic in $\boldsymbol{\lambda}$, hence

$$\mathbf{f}^{(1)}(+\boldsymbol{\lambda}) = \mathbf{f}^{(1)}(-\boldsymbol{\lambda}) \tag{95}$$

If we consider a porous medium that verifies the reversibility assumption (Eq. 22), as in Firdaouss et al. (1997), we have at order 1

$$\underbrace{-\epsilon_\beta v\left[\mathbf{K}_{\boldsymbol{D}}^{-1}\cdot(-\boldsymbol{\lambda})+\mathbf{f}^{(1)}(-\boldsymbol{\lambda})\delta+O\left(\delta^2\right)\right]}_{\mathbf{g}_\beta(-\boldsymbol{\lambda},v)}=\underbrace{-\left(-\epsilon_\beta v\left[\mathbf{K}_{\boldsymbol{D}}^{-1}\cdot(+\boldsymbol{\lambda})+\mathbf{f}^{(1)}(+\boldsymbol{\lambda})\delta+O\left(\delta^2\right)\right]\right)}_{-\mathbf{g}_\beta(+\boldsymbol{\lambda},v)}, \tag{96}$$

so that if our AGF equation is correct, we must have

$$\mathbf{f}^{(1)}(-\lambda)=-\mathbf{f}^{(1)}(+\lambda), \tag{97}$$

which implies that $\mathbf{f}^{(1)}=0$, or equivalently

$$F_{\parallel}^{(1)}=F_{\perp}^{(1)}=0. \tag{98}$$

We have already shown that our asymptotic development yields $F_{\parallel}^{(1)}=0$ for any periodic porous media. Hence, the new information in Eq. 98 is that $F_{\perp}^{(1)}$ must be zero for our AGF expression to be valid in porous media where the reversibility assumption is verified. Interestingly, Eq. 91 does not allow to conclude (to our knowledge) that $F_{\perp}^{(1)}=0$ when $d=\boldsymbol{\lambda}^{\perp}$ a direction orthogonal to the flow direction $\boldsymbol{\lambda}$, and yet, this has to be the case under the reversibility assumption.

References

Agnaou, M., Lasseux, D., Ahmadi, A.: From steady to unsteady laminar flow in model porous structures: an investigation of the first hopf bifurcation. Comput. Fluids **136**, 67–82 (2016)

Amiri, A., Vafai, K.: Analysis of dispersion effects and non-thermal equilibrium, non-Darcian, variable porosity incompressible flow through porous media. Int. J. Heat Mass Transf. **37**(6), 939–954 (1994)

Andrade Jr., J.S., Street, D.A., Shinohara, T., Shibusa, Y., Arai, Y.: Percolation disorder in viscous and non-viscous flow through porous media. Phys. Rev. E **51**(6), 5725 (1995)

Andrade Jr., J.S., Costa, U.M.S., Almeida, M.P., Makse, H.A., Stanley, H.E.: Inertial effects on fluid flow through disordered porous media. Phys. Rev. Lett. **82**(26), 5249 (1999)

Antohe, B.V., Lage, J.L.: A general two-equation macroscopic turbulence model for incompressible flow in porous media. Int. J. Heat Mass Transf. **40**(13), 3013–3024 (1997)

Aydın, O., Kaya, A.: Non-Darcian forced convection flow of viscous dissipating fluid over a flat plate embedded in a porous medium. Transport Porous Media **73**(2), 173–186 (2008)

Beavers, G.S., Sparrow, E.M.: Non-Darcy Flow Through Fibrous Porous Media. American Society of Mechanical Engineers, New York (1969)

Brace, W.F., Walsh, J.B., Frangos, W.T.: Permeability of granite under high pressure. J. Geophys. Res. **73**(6), 2225–2236 (1968)

Carman, P.C.: Fluid flow through granular beds. Chem. Eng. Res. Design **15**, 150–166 (1937)

Chandesris, M., Serre, G., Sagaut, P.: A macroscopic turbulence model for flow in porous media suited for channel, pipe and rod bundle flows. Int. J. Heat Mass Transf. **49**(15), 2739–2750 (2006)

Chauveteau, G., Thirriot, C.: Régimes d'écoulement en milieu poreux et limite de la loi de Darcy. La Houille Blanche (2), 141–148 (1967)

Chikhi, N., Clavier, R., Laurent, J.-P., Fichot, F., Quintard, M.: Pressure drop and average void fraction measurements for two-phase flow through highly permeable porous media. Ann. Nucl. Energy **94**, 422–432 (2016)

Clavier, R.: Étude expérimentale et modélisation des pertes de pression lors du renoyage d'un lit de débris. Ph.D. thesis, Institut National Polytechnique de Toulouse, France (2015)

Clavier, R., Chikhi, N., Fichot, F., Quintard, M.: Experimental investigation on single-phase pressure losses in nuclear debris beds: identification of flow regimes and effective diameter. Nucl. Eng. Design **292**, 222–236 (2015)

Clavier, R., Chikhi, N., Fichot, F., Quintard, M.: Experimental study of single-phase pressure drops in coarse particle beds. Nucl. Eng. Design **312**, 184–190 (2017)

Darcy, H.: Les fontaines publiques de la ville de Dijon. Victor Dalmont, Paris (1856)
Davit, Y., Quintard, M.: Technical notes on volume averaging in porous media I: how to choose a spatial averaging operator for periodic and quasiperiodic structures. Transport Porous Media **119**, 1–30 (2017)
de Carvalho, T.P., Morvan, H.P., Hargreaves, D.M., Oun, H., Kennedy, A.: Pore-scale numerical investigation of pressure drop behaviour across open-cell metal foams. Transport in Porous Media **117**, 1–26 (2017)
De Lemos, M.J.: Turbulence in Porous Media: Modeling and Applications. Elsevier, Oxford (2012)
Dukhan, N., Bağcı, Ö., Özdemir, M.: Experimental flow in various porous media and reconciliation of Forchheimer and Ergun relations. Exp. Therm. Fluid Sci. **57**, 425–433 (2014)
Dybbs, A., Edwards, R.: A new look at porous media fluid mechanics-Darcy to turbulent. In: Bear, J., Corapcioglu, M.Y. (eds.) Fundamentals of Transport Phenomena in Porous Media, pp. 199–256. Springer, Berlin (1984)
Ergun, S.: Fluid flow through packed columns. Chem. Eng. Prog. **48**, 89–94 (1952)
Fand, R., Kim, B., Lam, A., Phan, R.: Resistance to the flow of fluids through simple and complex porous media whose matrices are composed of randomly packed spheres. J. Fluids Eng. **109**(3), 268–274 (1987)
Favier, J., Dauptain, A., Basso, D., Bottaro, A.: Passive separation control using a self-adaptive hairy coating. J. Fluid Mech. **627**, 451–483 (2009)
Firdaouss, M., Guermond, J.-L., Le Quéré, P.: Nonlinear corrections to Darcy's law at low Reynolds numbers. J. Fluid Mech. **343**, 331–350 (1997)
Forchheimer, P.H.: Wasserbewegung durch boden. Z. Vereines Dtsch. Ing. **45**, 1782–1788 (1901)
Ghisalberti, M., Nepf, H.: Mixing layers and coherent structures in vegetated aquatic flows. J. Geophys. Res. **107**(C2), 420 (2002)
Ghisalberti, M., Nepf, H.: Mass transport in vegetated shear flows. Environ. Fluid Mech. **5**(6), 527–551 (2005)
Gosselin, F.: Mécanismes d'interactions fluide-structure entre écoulements et végétation. Ph.D. thesis, École Polytechnique (2009)
Gosselin, F.P., de Langre, E.: Drag reduction by reconfiguration of a poroelastic system. J. Fluids Struct. **27**, 1111–1123 (2011)
Goyeau, B., Songbe, J.-P., Gobin, D.: Numerical study of double-diffusive natural convection in a porous cavity using the Darcy-Brinkman formulation. Int. J. Heat Mass Transf. **39**(7), 1363–1378 (1996)
Hassanizadeh, S.M., Gray, W.G.: High velocity flow in porous media. Transport Porous Media **2**(6), 521–531 (1987)
Hlushkou, D., Tallarek, U.: Transition from creeping via viscous-inertial to turbulent flow in fixed beds. J. Chromatogr. A **1126**(1), 70–85 (2006)
Hoffmann, J., Echigo, R., Yoshida, H., Tada, S.: Experimental study on combustion in porous media with a reciprocating flow system. Combust. Flame **111**(1–2), 32–46 (1997)
Hong, J., Yamada, Y., Tien, C.: Effects of non-darcian and nonuniform porosity on vertical-plate natural convection in porous media. J. Heat Transf. **109**(2), 356–362 (1987)
Jackson, G.W., James, D.F.: The permeability of fibrous porous media. Can. J. Chem. Eng. **64**(3), 364–374 (1986)
Jin, Y., Kuznetsov, A.V.: Turbulence modeling for flows in wall bounded porous media: an analysis based on direct numerical simulations. Phys. Fluids **29**(4), 045102 (2017)
Jin, Y., Uth, M., Kuznetsov, A., Herwig, H.: Numerical investigation of the possibility of macroscopic turbulence in porous media: a direct numerical simulation study. J. Fluid Mech. **766**, 76 (2015)
Kim, S.Y., Paek, J.W., Kang, B.H.: Flow and heat transfer correlations for porous fin in a plate-fin heat exchanger. J. Heat Transf. **122**(3), 572–578 (2000)
Klinkenberg, L.J.: The permeability of porous media to liquids and gases. In: Drilling and Production Practice. American Petroleum Institute, Washington (1941)
Koch, D.L., Ladd, A.J.C.: Moderate Reynolds number flows through periodic and random arrays of aligned cylinders. J. Fluid Mech. **349**, 31–66 (1997)
Kuwahara, F., Kameyama, Y., Yamashita, S., Nakayama, A.: Numerical modeling of turbulent flow in porous media using a spatially periodic array. J. Porous Media **1**(1), 47–55 (1998)
Lage, J.L.: The fundamental theory of flow through permeable media from Darcy to turbulence. In: Ingham, D.B., Pop, I. (eds.) Transport Phenomena in Porous Media, pp. 1–30. Elsevier, Oxford (1998)
Lage, J.L., Antohe, B.V.: Darcy's experiments and the deviation to nonlinear flow regime. J. Fluids Eng. **122**(3), 619–625 (2000)
Lasseux, D., Valdés-Parada, F.J.: On the developments of Darcy's law to include inertial and slip effects. Compt. Rendus Méc. **345**(9), 660–669 (2017)
Lasseux, D., Abbasian Arani, A.A., Ahmadi, A.: On the stationary macroscopic inertial effects for one phase flow in ordered and disordered porous media. Phys. Fluids **23**(7), 073103 (2011)
Li, L., Ma, W.: Experimental study on the effective particle diameter of a packed bed with non-spherical particles. Transport Porous Media **89**(1), 35–48 (2011a)

Li, L., Ma, W.: Experimental characterization of the effective particle diameter of a particulate bed packed with multi-diameter spheres. Nucl. Eng. Design **241**(5), 1736–1745 (2011b)
Lucas, Y., Panfilov, M., Buès, M.: High velocity flow through fractured and porous media: the role of flow non-periodicity. Eur. J. Mech. B/Fluids **26**(2), 295–303 (2007)
Luminari, N., Airiau, C., Bottaro, A.: Effects of porosity and inertia on the apparent permeability tensor in fibrous media. Int. J. Multiph. Flow **106**, 60–74 (2018)
Ma, H., Ruth, D.: Physical explanations of non-Darcy effects for fluid flow in porous media. SPE Form. Eval. **12**(01), 13–18 (1997)
Masuoka, T., Takatsu, Y.: Turbulence model for flow through porous media. Int. J. Heat Mass Transf. **39**(13), 2803–2809 (1996)
Mcdonald, I.F., El-Sayed, M.S., Mow, K., Dullien, F.A.L.: Flow through porous media-the Ergun equation revisited. Ind. Eng. Chem. Fundam. **18**(3), 199–208 (1979)
Mei, C.C., Auriault, J.L.: The effect of weak inertia on flow through a porous medium. J. Fluid Mech. **222**, 647–663 (1991)
Muljadi, B.P., Blunt, M.J., Raeini, A.Q., Bijeljic, B.: The impact of porous media heterogeneity on non-Darcy flow behaviour from pore-scale simulation. Adv. Water Resour. **95**, 329–340 (2016)
Nakayama, A., Kuwahara, F.: A macroscopic turbulence model for flow in a porous medium. J. Fluids Eng. **121**, 427–433 (1999)
Nield, D.A., Bejan, A.: Convection in Porous Media. Springer, New York (1999)
Panfilov, M., Oltean, C., Panfilova, I., Buès, M.: Singular nature of nonlinear macroscale effects in high-rate flow through porous media. Compt. Rendus Méc. **331**(1), 41–48 (2003)
Papathanasiou, T.D., Markicevic, B., Dendy, E.D.: A computational evaluation of the Ergun and Forchheimer equations for fibrous porous media. Phys. Fluids **13**(10), 2795–2804 (2001)
Philipse, A.P., Schram, H.L.: Non-Darcian airflow through ceramic foams. J. Am. Ceram. Soc. **74**(4), 728–732 (1991)
Quintard, M., Whitaker, S.: Transport in ordered and disordered porous media II: generalized volume averaging. Chem. Eng. Sci. **14**, 179–206 (1994a)
Quintard, M., Whitaker, S.: Transport in ordered and disordered porous media III: closure and comparison between theory and experiment. Chem. Eng. Sci. **15**, 31–49 (1994b)
Quintard, M., Kaviany, M., Whitaker, S.: Two-medium treatment of heat transfer in porous media: numerical results for effective properties. Adv. Water Resour. **20**(2), 77–94 (1997)
Rojas, S., Koplik, J.: Nonlinear flow in porous media. Phys. Rev. E **58**, 4776–4782 (1998)
Ruth, D., Ma, H.: On the derivation of the Forchheimer equation by means of the averaging theorem. Transport Porous Media **7**(3), 255–264 (1992)
Schneebeli, G.: Expériences sur la limite de validité de la loi de Darcy et l'apparition de la turbulence dans un écoulement de filtration. La Houille Blanche (2), 141–149 (1955)
Seguin, D., Montillet, A., Comiti, J.: Experimental characterisation of flow regimes in various porous media. I: limit of laminar flow regime. Chem. Eng. Sci. **53**(21), 3751–3761 (1998a)
Seguin, D., Montillet, A., Comiti, J., Huet, F.: Experimental characterization of flow regimes in various porous media. II: transition to turbulent regime. Chem. Eng. Sci. **53**(22), 3897–3909 (1998b)
Sharp, K.V., Adrian, R.J.: Transition from laminar to turbulent flow in liquid filled microtubes. Exp. Fluids **36**(5), 741–747 (2004)
Skjetne, E., Auriault, J.L.: New insights on steady, nonlinear flow in porous media. Eur. J. Mech. B/Fluids **18**(1), 131–145 (1999)
Souto, H.P.A., Moyne, C.: Dispersion in two-dimensional periodic porous media. Part I: hydrodynamics. Phys. Fluids **9**(8), 2243–2252 (1997)
Vafai, K., Tien, C.L.: Boundary and inertia effects on flow and heat transfer in porous media. Int. J. Heat Mass Transf. **24**(2), 195–203 (1981)
Vafai, K., Tien, C.: Boundary and inertia effects on convective mass transfer in porous media. Int. J. Heat Mass Transf. **25**(8), 1183–1190 (1982)
Venkataraman, P., Rao, P.R.M.: Darcian, transitional, and turbulent flow through porous media. J. Hydraul. Eng. **124**(8), 840–846 (1998)
Whitaker, S.: Diffusion and dispersion in porous media. Am. Inst. Chem. Eng. **13**(3), 420–427 (1967)
Whitaker, S.: The Forchheimer equation: a theoretical development. Transport Porous Media **25**(1), 27–61 (1996)
Whitaker, S.: The Method of Volume Averaging. Kluwer Academic, Dordrecht (1999)
Wodie, J.-C., Levy, T.: Correction non linéaire de la loi de Darcy. Comptes Rendus de l'Académie des Sciences. Série 2, Mécanique, Physique, Chimie, Sciences de l'Univers Sciences de la Terre **312**(3), 157–161 (1991)
Wong, T.-F., David, C., Zhu, W.: The transition from brittle faulting to cataclastic flow in porous sandstones: mechanical deformation. J. Geophys. Res. Solid Earth **102**(B2), 3009–3025 (1997)

Wood, B.D.: Inertial effects in dispersion in porous media. Water Resour. Res. **43**(12), W12S16 (2007)
Zeng, Z., Grigg, R.: A criterion for non-Darcy flow in porous media. Transport Porous Media **63**(1), 57–69 (2006)
Zimmerman, R.W., Al-Yaarubi, A., Pain, C.C., Grattoni, C.A.: Nonlinear regimes of fluid flow in rock fractures. Int. J. Rock Mech. Min. Sci. **41**, 163–169 (2004)